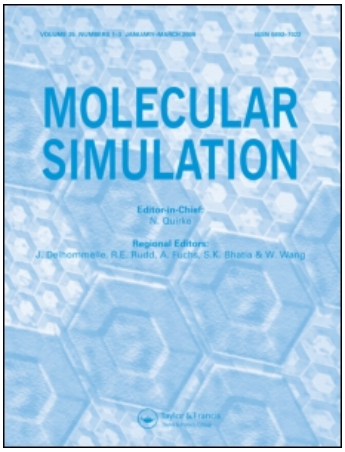

Molecular Simulation
Publication details, including instructions for authors and subscription information:
http://www.informaworld.com/smpp/title~content=t713644482

Simulation of a Hard-Sphere Fluid in Bicontinuous Random Media

I. -A. Park[a]; J. M. D. Macelroy[a]
[a] Department of Chemical Engineering, University of Missouri-Rolla, Rolla, Missouri, USA

To cite this Article Park, I. -A. and Macelroy, J. M. D.(1989) 'Simulation of a Hard-Sphere Fluid in Bicontinuous Random Media', Molecular Simulation, 2: 1, 105 — 145
To link to this Article: DOI: 10.1080/08927028908032786
URL: http://dx.doi.org/10.1080/08927028908032786

Molecular Simulation, 1989, Vol. 2, pp. 105–145
Reprints available directly from the publisher
Photocopying permitted by license only

SIMULATION OF A HARD-SPHERE FLUID IN BICONTINUOUS RANDOM MEDIA

I.-A. PARK and J.M.D. MacELROY

Department of Chemical Engineering, University of Missouri-Rolla, Rolla, Missouri 65401, USA

(*Received January 1988; in final form April 1988*)

The influence of solid-phase connectivity on size-exclusion partitioning and on diffusion of a dilute hard-sphere fluid in overlapping and nonoverlapping spheres models of porous media is investigated using molecular dynamics and Monte Carlo simulation techniques. Four models are examined, two of which are subject to constrained bicontinuity of the pore and solid phases and two in which the solid spheres in the assemblies are randomly distributed in space. It is shown that at moderate to high porosities, connected (bicontinuous) structures lead to a significant increase in the partition and diffusion coefficients when the particles of the pore fluid are of finite size. The consequences of solid phase connectivity are also clearly illustrated in the long-time decay of the velocity autocorrelation function (VACF) of the diffusing particles, particularly in the vicinity of the percolation threshold. Under these conditions the power law exponents on the long-time tail of the VACF are generally found to be higher in connected models than in random systems and the importance of this result is demonstrated using one of the scaling rules of percolation theory. The simulation results are also compared with the predictions of current theories of partitioning and diffusion in random sphere assemblies and, with reference to experimental data available from the literature, it is shown that bicontinuous models are better representations of real porous media.

KEY WORDS: Lorentz gases, diffusion, partitioning, percolation, porous media

1 INTRODUCTION

In the development of an accurate theory for partitioning and diffusion in solid/fluid composites, one of the major difficulties encountered lies in the description of the structure of the solid phase and the topology of the pore space [1]. For crystalline media (e.g. zeolites) this is not a serious problem; however, in many industrial processes the porous substrates or membranes employed are amorphous with complicated random internal structures. A specific class of models for such systems which has enjoyed popularity in recent years views the structure of two-phase composites as inclusions (spherical or nonspherical) randomly distributed in space [2—13]. The inclusions are usually treated as the solid phase ("cannonball" solid) with the interinclusion void space as the distributing phase. The converse ("swiss cheese") construction has also received attention.

In this paper we report computer simulation results for four different models of cannonball solids in which, as the name implies, the solid inclusions are considered to be spherical. The models investigated are (i) random overlapping spheres, (ii) randomly connected overlapping spheres, (iii) random nonoverlapping spheres, and

(iv) randomly connected nonoverlapping spheres. In each case the solid spheres are uniform in size with radius σ_s as illustrated schematically in Figure 1. Current theoretical results for sphere assemblies only apply for models (i) and (iii) although in reality the solid phase of any porous medium is continuous in a manner similar to that suggested by models (ii) and (iv).

The distinction between models (i) and (ii) primarily arises in the range of void fractions $\psi > 0.5$ since we may infer from static percolation studies on lattice and continuum structures [14–16] that the random overlapping system (model (i)) is fully connected below $\psi = 0.5$. For porosities in the range $\psi > 0.5$, however, isolated clusters of solid spheres, as illustrated for the simple case of a single particle in Figure 1(a), are permitted in the unbiased random model and these small clusters are dominant above the known percolation threshold ($\psi = 0.71$) for this system [14–16].

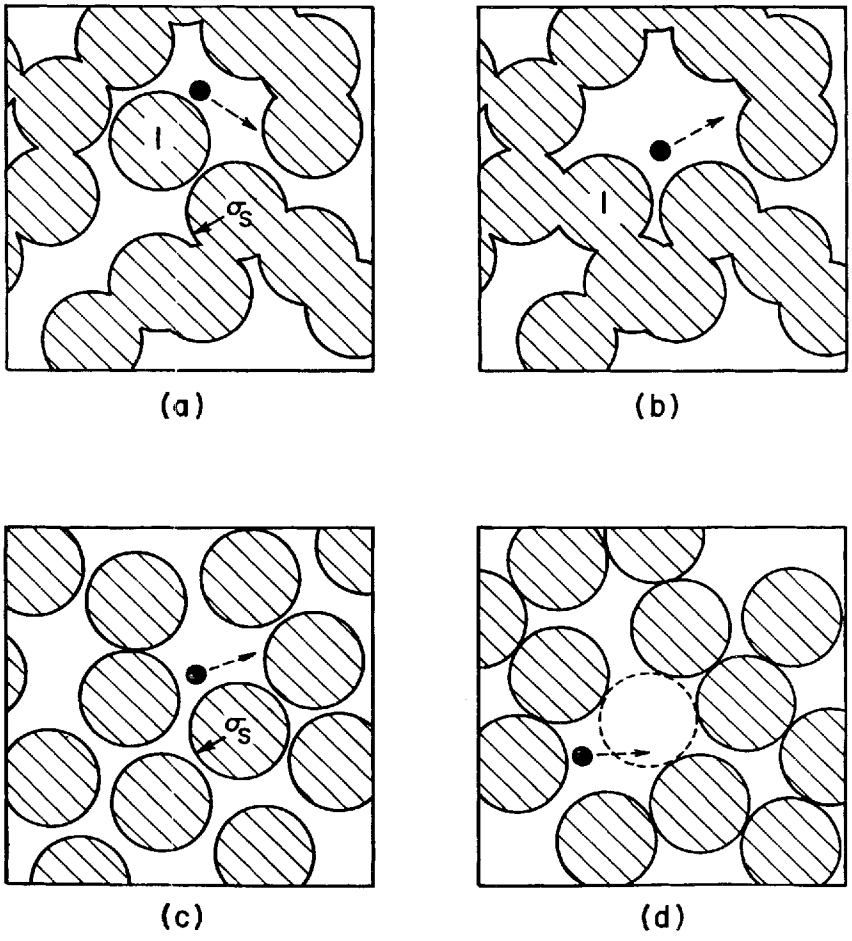

Figure 1 Schematic representations of overlapping and nonoverlapping spheres models. (a) Model (i); (b) model (ii); (c) model (iii); (d) model (iv). The shaded regions represent the solid phase and the full circle corresponds to a fluid particle moving through the void space generated in each case.

As outlined in the Appendix, the method employed here to generate assemblies of the type shown in Figure 1(b) ensures that the individual solid spheres overlap with at least one or more of the other spheres in the system in such a way that only one macroscopically connected cluster exists regardless of the porosity of the medium. One of the objectives of this study is to show that the transition from the natural connectivity of model (i) at low porosities to the constrained connectivity of model (ii) for $\psi > 0.5$ has very important consequences when the particles of the diffusing fluid within the pore space have a size commensurate with the characteristic void dimensions of the medium.

In contrast to the overlapping models, solid phase connectivity in the random nonoverlapping system only exists when the individual spheres in the structure are in pointwise contact with one or more nearest neighbors (Figure 1(d)). Here we employ the basic premise that a random close-packed (RCP) structure [17–19] of porosity $\psi = 0.367$ is fully connected (our definition of connectivity in this case is discussed in the Appendix) and that nonoverlapping connected sphere systems of higher porosity can be generated by randomly removing spheres from the RCP structure with subsequent elimination of small isolated clusters. The topological properties of these connected models are quite different from the random nonoverlapping system at moderate to high porosities since connectivity is never truly guaranteed in the latter case except possibly below $\psi = 0.44$ (very loose random packing [20]). For random compacts of the type shown in Figure 1(d) with holes generated by removal of spheres (one such hole is schematically illustrated as an unshaded dashed circle) Kirkpatrick [15] has shown that the percolation threshold for continuity of the solid phase occurs at a void fraction $\psi = 0.75$. Although this porosity does not necessarily represent the upper limit attainable for the connected nonoverlapping system since isolated clusters of spheres are discarded during the construction of the model, here we restrict our studies to porosities less than 0.75.

To demonstrate the influence of the topology of the solid on diffusion and percolation we have conducted molecular dynamics (MD) simulations for one of the simplest known pore fluid models, namely a single hard-sphere particle moving through the pore space generated by models (i) through (iv) as illustrated in Figure 1. The steady-state diffusion flux for isolated particles in these systems is given by Fick's law

$$\mathbf{J} = -D\nabla n \tag{1}$$

where D is the diffusion coefficient and n is the local number density of the diffusing particles. The number density n refers to unit volume of the medium and is related, through the assumption of local equlibrium, to a corresponding density, n_0, for a phase devoid of inclusions,

$$n = \psi K n_0 \tag{2}$$

where ψ is the total porosity of the medium and K is the equilibrium partition coefficient.

Solid/fluid systems of the type described above are generally referred to as Lorentz gases [21] and are representative of the limiting condition of Knudsen diffusion in porous media. Recent molecular dynamics studies of Lorentz gases [22–27] have been primarily concerned with two-dimensional random overlapping or nonoverlapping disk systems although in the earlier work of Bruin [22] results obtained from a limited number of simulations of the three-dimensional random overlapping spheres model

were reported. The MD simulation runs conducted in the present studies are two orders of magnitude longer than Bruin's and our improved statistics will allow for a more detailed assessment of the predictions of contemporary Lorentz gas kinetic theory away from and near the percolation threshold [28–35].

The emphasis of this paper will be on diffusion in models (i) through (iv); however, we will also present results for equilibrium partitioning obtained using a straightforward Monte Carlo procedure coupled with a modification of the particle trajectory method described by Nakano and Evans [6]. These results will provide a basis for comparison with current theories for equilibrium partitioning in random sphere assemblies [4, 10, 11].

In Section 2, the results of the simulations of the random overlapping and high porosity connected overlapping systems will be presented. The discussion will be preceded by a brief outline of the reduced units employed and the reader is referred to the Appendix for details of the simulation methods used. The format for the presentation of the results for the nonoverlapping systems in Section 3 will be similar, and a description of the simulation procedures employed is also provided in the Appendix. A summary and conclusions are given in Section 4.

2 OVERLAPPING SYSTEMS

In all of the simulations reported here and for the nonoverlapping structures to be discussed in Section 3 the moving gas particle is assumed to undergo elastic, specular scattering during collisions with the stationary solid spheres. The kinetic energy of the particle and hence its speed, v, are constant. v and the solid sphere radius σ_s are therefore the primary quantities used in the reduction of units. In particular we define the reduced diffusion coefficient

$$D^* = D/v\sigma_s = \lim_{t^* \to \infty} (\tau_c^*/3) \int_0^{t^*} d\tau^* \, C(\tau^*) \tag{3a}$$

$$= \lim_{t^* \to \infty} (1/6\tau_c^*) \frac{d}{dt^*} \langle (\mathbf{r}^*(t^*) - \mathbf{r}^*(0))^2 \rangle \tag{3b}$$

Equation (3a) is the Green-Kubo relation and Equation (3b) is the Einstein equation [36]. $C(\tau^*)$ is the normalized velocity autocorrelation function (VACF)

$$C(\tau^*) = \langle \mathbf{v}(0) \cdot \mathbf{v}(\tau^*) \rangle / \langle v^2 \rangle \tag{4}$$

and the dimensionless times τ^* and t^* are in units of the mean free time τ_c. $\mathbf{r}^*(t^*)$ in Equation (3b) is the position of the diffusing particle at time t^* reduced by σ_s.

For overlapping systems the appropriate collision time, τ_c, is the Boltzmann mean free time which is given by

$$\tau_c(v/\sigma_s) = \tau_B^* = 1/(\pi n_s^* (1 + \sigma)^2) \tag{5}$$

where n_s^* is the number density of the solid spheres (scattering centers) reduced by σ_s^3 and σ is the radius of the moving particle reduced by σ_s. Equation (5) is exact for random overlapping systems but understimates the mean collision time in connected structures above $\psi = 0.5$ as will be seen below.

Another quantity which will be used during the presentation of the results is the Boltzmann diffusion coefficient D_B^* for completely random systems

$$D_B^* = 1/(3\pi n_s^* (1 + \sigma)^2) \tag{6}$$

Equation (6) follows from Equation (3a) when the VACF is assumed to decay exponentially according to the expression

$$C(t^*) = \exp(-t^*)$$

This simple decay is now known to be inexact, even at low densities, and the precise form of $C(t^*)$, particularly at long times, is one of the major issues of modern kinetic theory. Indeed, as we will see below, the behaviour of the long-time tail in the VACF plays a key role in the investigation of diffusional phenomena in two-phase random media, particularly in the vicinity of the percolation threshold where the concept of anomalous diffusion in percolation theory (see for example [37]) enters into the analysis.

In all of the simulations conducted on the random overlapping spheres model (model (i)) the isolated diffusing particle was treated as a point of zero radius. However, our results can be interrelated to diffusing particles of finite size through the simple expression [3]

$$\psi = \exp(-\frac{4}{3}\pi n_s^* (1 + \sigma)^3) \tag{7}$$

where ψ is the total porosity of the medium. Equation (7) may also be used to define the partition coefficient in the random overlapping system

$$\begin{aligned} K &= PK_T \\ &= P\psi^{(1+\sigma)^3 - 1} \end{aligned} \tag{8}$$

where P is the percolation probability of the medium and K_T is the partition coefficient referred to the total porosity ψ [4]. This equation will be employed later during the presentation of the Monte Carlo simulation results for partitioning in the high porosity connected system (model (ii)). We start the discussion however by first considering the dynamical properties of the random overlapping Lorentz gas since this model has been widely studied in recent years.

2.1 Results for Model (i)

In Figure 2(a) we illustrate the VACF's obtained at several porosities for the random overlapping system. The structure of the VACF at short times does not differ significantly from the results obtained earlier by Bruin [22]; however, in Figures 2(b) through 2(d) we show long-time tails not accessible to Bruin due to the limited statistics involved in his simulations. Current theories of diffusion in the random overlapping Lorentz gas [30–35] predict a power law decay of the VACF tail given by

$$C(t^*) = -\frac{\alpha}{t^{*\beta}} \tag{9}$$

where α is a density dependent coefficient. For low to moderate densities (high porosity) all theories are consistent in the prediction that the power law exponent β is 2.5. Differences arise however in the theoretical results for α as a function of density and also for β at high densities. The results we obtained from least-squares analysis of the VACF tails using Equation (9) are given in Table 1. Within statistical error the

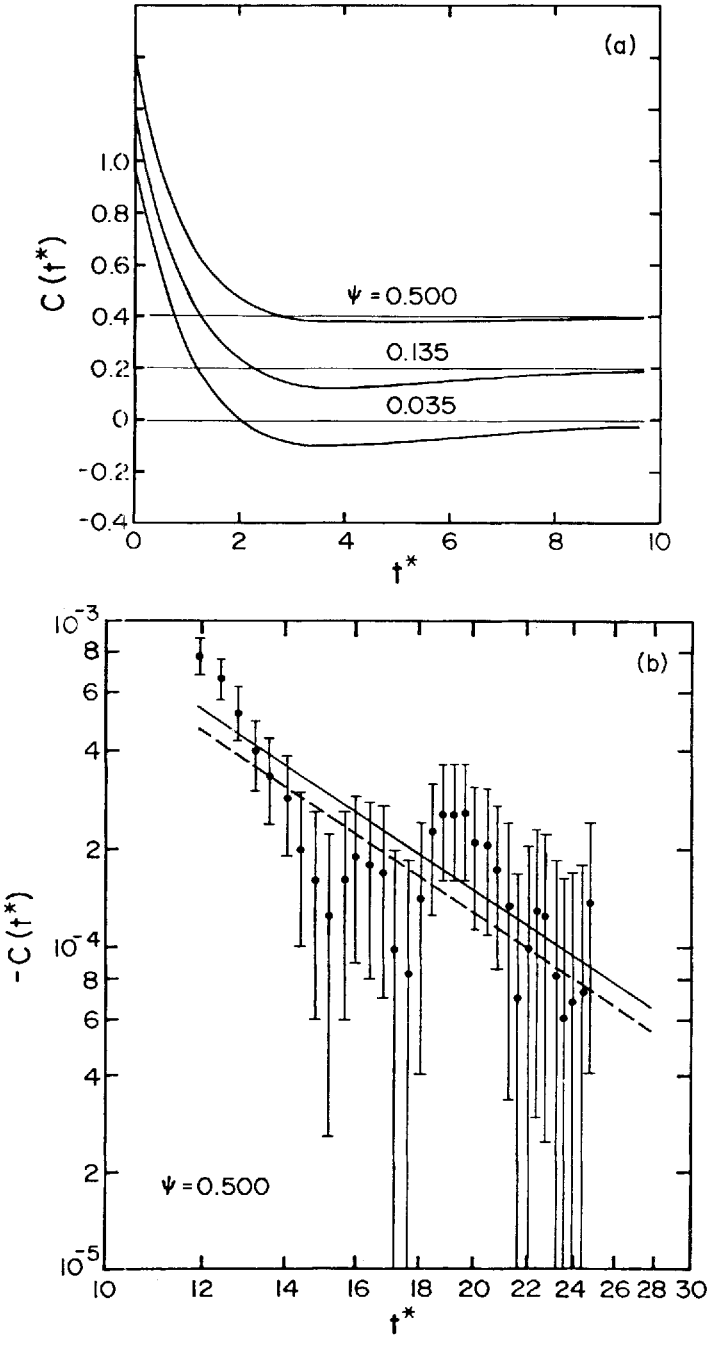

Figure 2 (a, b) Normalized velocity autocorrelation function for the random overlapping system. (a) Short time behaviour for several porosities. (b) The long-time tail for $\psi = 0.5$. ● MD simulation; ——— fit to a $t^{*-2.5}$ power law decay; - - - - mode-coupling theory of Ernst *et al.* [34, 35].

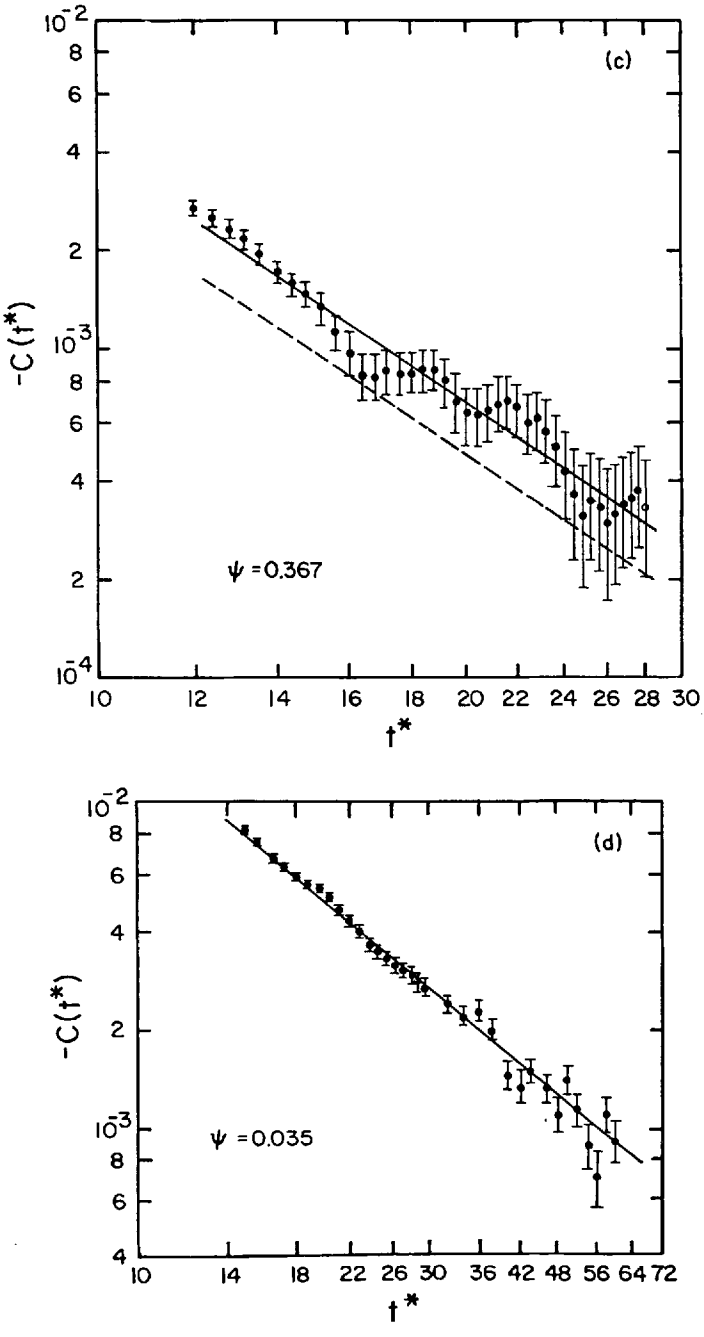

Figure 2 (c, d) (c) As in (b) but for $\psi = 0.367$. (d) The long-time tail for $\psi = 0.035$. ● MD simulation; —— least squares fit to a $t^{*-\beta}$ power law decay ($\beta = 1.57$).

Table 1 Parameters for the Long-Time Tails of the VACF. Random Overlapping System.

ψ	(n_s^*)	N_s^a	$N_c^b(10^3)$	$N_{col}^c(10^3)$	Δt^{*d}	α^e	β^e
0.644	(0.105)	400	5.0	2.0		–	–
0.500	(0.165)	200	15.0	2.0	12–25	0.09(4)	2.2(2)
						0.26(8)	2.5
0.367	(0.239)	200	10.0	2.0	12–25	1.1(2)	2.47(8)
						1.2(2)	2.5
0.250	(0.331)	200	6.0	2.0	15–30	0.8(2)	1.77(8)
0.185	(0.403)	200	5.0	2.0	15–30	0.62(5)	1.77(3)
0.135	(0.477)	200	1.5	6.0	15–30	0.59(4)	1.66(2)
0.080	(0.603)	400	1.5	16.0	15–40	0.59(3)	1.58(2)
		200	1.0	10.0	15–40	0.58(4)	1.59(2)
0.060	(0.672)	400	1.5	16.0	15–40	0.55(2)	1.55(1)
0.0498	(0.716)	400	1.5	16.0	15–40	0.62(3)	1.60(2)
		200	1.5	10.0	15–40	0.65(5)	1.62(3)
0.0425	(0.754)	400	1.5	16.0	15–40	0.61(4)	1.60(2)
0.035	(0.800)	400	1.5	16.0	15–40	0.55(4)	1.57(2)
		200	1.5	10.0	15–40	0.53(3)	1.59(2)

[a] N_s is the number of scattering centers.
[b] N_c is the total number of configurations generated.
[c] N_{col} is the total length of the trajectory, in Boltzmann mean free times, for any given configuration.
[d] Δt^* is the time range, in Boltzmann collision times, employed in the least-squares fit of the tail.
[e] The second set of results for $\psi = 0.500$ and 0.367 were obtained from a fit to $t^{*-2.5}$.
[f] This run was of insufficient length to determine α and β with any accuracy.

values for β at porosities $\psi = 0.5$ and 0.367 are in agreement with the value 2.5 and the full lines shown in Figures 2(b) and 2(c) correspond to the second set of parameters given in Table 1 for these porosities. In Figures 2(b) and 2(c) we also show the tails predicted by the mode-coupling theory of Ernst *et al.* [34, 35]. This theory was found to be superior to the earlier theoretical results for α proposed by Keyes and Mercer [30] and Gotze *et al.* [31]. The approximate expression for α given by Ernst *et al.* is

$$\alpha = \frac{(3\pi)^{1.5} n_s^{*2}}{16} \left[\frac{d \ln D^*}{d \ln n_s^*} + \ln \psi \right]^2 \left(\frac{D_B}{D} \right)^{1.2} \tag{10}$$

The derivative appearing in this equation has been calculated by fitting the results for D^* in Table 2 to a simple function of n_s^* in the range $n_s^* < 0.3$. The values for α so obtained were 0.23 and 0.84 for $\psi = 0.5$ and 0.367 respectively and, as the dashed lines in Figures 2(b) and 2(c) demonstrate, are in fair agreement with the MD tails. The result for $\psi = 0.5$ is in fact well within the error bounds on the simulation data and lend strong support to the mode-coupling method, at least for the three-dimensional studies considered here. At the higher density the agreement is not as good due, possibly, to the neglect of a term appearing in the general mode-coupling result for α [34] which involves fluctuations in the orthogonal part of the local (spatially dependent) diffusivity tensor. As discussed by Machta *et al.* [35], this neglected contribution cannot be readily evaluated due to the nonthermodynamic nature of the fluctuations involved.

As the porosity of the medium is decreased, the results given in Table 1 show that the coefficient α first increases and then decreases to an average value of approximately 0.58. (There appears to be a local maximum in α at $\psi = 0.0498$ and, as will be seen below, this is a feature common to all of the systems investigated here as the percolation threshold is approached). The power law exponent β is also seen to

Table 2 Simulation Results for the Random Overlapping System.

ψ	N_s^a	D^{*b}	ψ_0/ψ^c	R_p^{*d}	τ_c^*/τ_B^{*e}
0.644	400	0.871(2)	1.0	1.589	1.00(1)
0.500	200	0.494(1)	1.0	1.004	1.00(1)
0.367	200	0.292(1)	1.0	0.696	1.00(1)
0.250	200	0.1616(6)	1.0	0.504	1.00(1)
0.185	200	0.1013(8)	1.0	0.409	0.99(2)
0.135	200	0.0610(6)	1.0	0.343	0.99(2)
0.080	400	0.0204(2)	0.995(4)	0.274	0.99(2)
	200	0.216(3)	0.990(5)	0.272	1.00(2)
0.060	400	0.0092(2)	0.93(1)	0.245	1.01(2)
0.0498	400	‡0.0046(2)	0.80(2)	0.231	1.01(2)
	200	‡0.0052(3)	0.79(2)	0.228	1.01(2)
0.0425	400	‡0.0022(2)	0.65(3)	0.217	0.99(2)
0.0350	400	‡−0.0002(3)	(0.49)	0.205	1.02(3)
	200	‡0.0004(3)	(0.56)	0.203	0.99(3)

[a] As in Table 1.
[b] D^* is the reduced diffusion coefficient $D/v\sigma_s$.
[c] ψ_0/ψ is the open porosity relative to the total porosity of the system.
The results for $\psi = 0.035$ are believed to be significantly in error due to size effects.
[d] R_p^* is the mean pore radius determined from the trajectories.
[e] τ_c^* is the mean free time determined from the simulations and τ_B^* is the Boltzmann mean free time.
‡ These diffusion coefficients were obtained by extrapolation of the long-time tails given in Table 1.

decrease sharply reaching a value of 1.57 at the lowest porosity investigated. The simulated long-time tail and the least-squares fit of Equation (9) for this last run, $\psi = 0.035$, are illustrated in Figure 2(d).

The observed trends in α and β are in qualitative agreement with self-consistent theories for the random overlapping Lorentz gas at moderate to high densities [31–33]. In particular, the theoretical results reported by Gotze *et al.* [32] are in part supported by our simulation data in the following respects. Gotze *et al.* have shown that one may define a time window (in our case this is 15–30 or 15–40 mean free times) over which one will obtain apparent values for α and β varying with n_s^* in the manner shown in Table 1. For times longer than the upper limit on this window the tail of the VACF will gradually approach the hydrodynamic power law (i.e. Equation (9) with $\beta = 2.5$). As the percolation threshold is approached (from below with respect to n_s^* or from above with respect to ψ) Gotze *et al.* suggest that the time window may be increased indefinitely without any observed change in the values of α and β and at the percolation threshold the hydrodynamic tail will recede to infinity. These predictions are best considered in relation to Figure 3.

In Figure 3 we plot the time-dependent diffusion coefficients for a number of runs near the percolation threshold. These results were obtained from integration of the VACF up to times of the order of 150–300 collision times (full circles) and from the slope of the mean-square displacement (see for example Figure 4) for times ranging from 300 to 3000 collision times (open circles (400 scattering centers) and open squares (200 scattering centers)). The full lines in Figure 3 correspond to extrapolation of the VACF tails (Table 1) using Equations (3a) and (9), i.e.

$$D^*(t^*) = D^*(t_0^*) + \frac{\alpha\tau_c^*}{3(\beta\text{-}1)}\left(t^{*(1\text{-}\beta)} - t_0^{*(1\text{-}\beta)}\right) \tag{11}$$

where t_0^* is a reference time typically chosen to be 40 collision times.

For times $t^* \lesssim 200$ the results obtained for the 200 and 400 particle systems do not differ appreciably. At long times however this is no longer true. For the lowest porosity, $\psi = 0.035$, we observe a 40% reduction in the apparent long-time diffusion coefficient in going from the 200 to the 400 particle system. For larger systems it is expected that the time dependent diffusion coefficient in this case will approach the solid line given by Equation (11) and will coincide with this expression in the limit $N_s \to \infty$. We note that the porosity $\psi = 0.035$ is within the range of the percolation threshold obtained by Kertesz [38] using a Monte Carlo method (his critical porosity is 0.034 + 0.007). Direct extrapolation of Equation (11) using the tail parameters given in Table 1 provides a diffusion coefficient which is zero, within statistical error, as $t^* \to \infty$. The agreement between this result and the Kertesz estimate of the percolation threshold confirms one aspect of the behaviour of the long-time tail predicted by self-consistent theories of diffusion in the Lorentz gas.

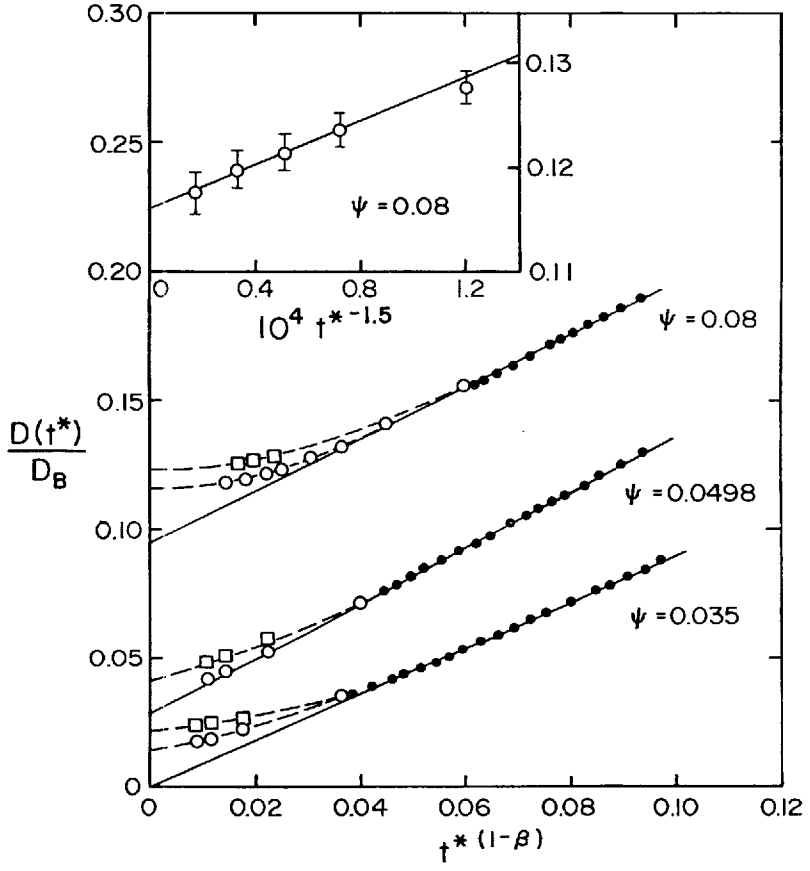

Figure 3 The time dependent diffusion coefficient for the random overlapping system near the percolation threshold. ● Results obtained from integration of the VACF; □, ○ results obtained from the long-time slope ($t^* > 300$) of the mean square displacement for $N_s = 200$ and 400 respectively. The power law exponents are: $\beta = 1.58$ ($\psi = 0.08$); 1.60 ($\psi = 0.0498$); 1.57 ($\psi = 0.035$). The inset shows a fit to an hydrodynamic power law at very long times ($500 < t^* < 1500$) for $\psi = 0.08$.

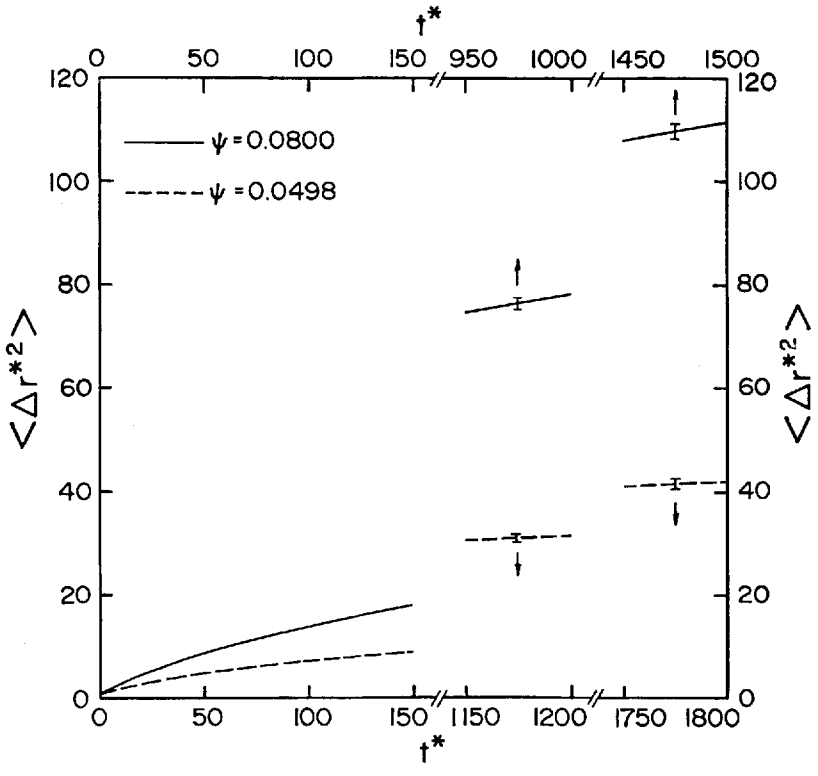

Figure 4 The mean square displacement as a function of time. —— $\psi = 0.08$; - - - - $\psi = 0.0498$.

As we move away from the percolation threshold the influence of size effects arising from density fluctuations is significantly reduced. The results shown in Figure 3 for $\psi = 0.0498$ in fact indicate that the 400 particle system is representative of the infinite system and also suggest that the infinite time diffusion coefficient may be obtained by extrapolation of Equation (11). In this case the 200 particle system gives a diffusion coefficient which is 30% too large. For the higher porosity, $\psi = 0.08$, we observe only a 6% difference between the two systems and for this reason we employed 200 scattering centers in nearly all of the runs at porosities $\psi > 0.08$ (Table 1 and 2). (For the case $\psi = 0.644$ a system containing 400 particles was considered more appropriate in order to reduce the possibility of channelling, i.e., collisionless motion of the gas particle as it passes through the fundamental cell).

The results shown in Figure 3 for $\psi = 0.08$ and for times $t^* > 250$ also appear to support another prediction of the theory proposed by Gotze *et al.* In this time range the diffusion coefficient displays a transition behaviour similar to that which one might expect as the power law exponent on the tail of the VACF changes from its value in the anomalous regime to the hydrodynamic value of 2.5. The inset in Figure 3 shows a least-squares fit of $D(t^*)/D_B$ to an hydrodynamic power law for the system $\psi = 0.08$, $N_s = 400$, over the time range $500 < t^* < 1500$, i.e., the four points at long times shown in the main diagram. The fifth point to the far right of the inset at

$t^* = 410$ is included to illustrate the minimum time needed to observe this apparent hydrodynamic tail.

The statements in the preceding paragraph need qualification since, as Alder and Alley [26] have noted in their discussion of long-time hydrodynamic tails in the two-dimensional Lorentz gas, due consideration must be given to the possible influence of system periodicity on the VACF tails at very long times. In fact they conclude from their results that hydrodynamic tails do not exist in moderate to high density Lorentz gases. In our high density system at $\psi = 0.08$ the upper time limit $t^* = 1500$ corresponds to a diffusion time scale which is approximately equal to the time required for the gas particle to move from one side to the opposite side of the fundamental cell. The influence of periodic boundary conditions therefore cannot be assumed negligible and this is apparent from the results obtained for the 200 particle system. This raises the following important questions: (a) Is the apparent hydrodynamic tail observed in Figure 3 solely a result of the finite "horizon" associated with periodic systems? (b) Are hydrodynamic long-time tails nonexistent as suggested by Alder and Alley? These questions lead to an additional problem: What is the correct extrapolation procedure one should use to obtain a reliable value for the diffusion coefficient as $t^* \to \infty$?

We have no conclusive answers to these questions; however, we do offer the following comments. To attempt to answer question (a) we can compare the results for $\psi = 0.08$ and 0.0498 shown in Figure 3. The long-time results for $\psi = 0.0498$ and $N_s = 400$ also correspond to the diffusion time scale for the system and these results do not appear to be seriously influenced by size effects. This would imply that the values for $D(t^*)$ at higher porosities may only be marginally affected by periodic boundary conditions for fundamental cells of the same size. If this is true then the long-time data for $\psi = 0.08$ may, in large part, reflect the influence of an hydrodynamic tail. This brings us to the contradiction posed by question (b), i.e., is there any reliable evidence to prove hydrodynamic tails exist. We believe we have convincing evidence for this for the nonoverlapping systems to be discussed later and this does not preclude the occurrence of these tails in the overlapping systems under consideration here. For this reason we feel that our results support the predictions of Gotze *et al.* [32] and that extrapolation of the long-time MD results for $\psi = 0.08$ in Figure 3 is favored over a direct extrapolation of the intermediate-time tail, as suggested by Alder and Alley [26], to obtain the infinite time diffusion coefficient. Our procedure may lead to slight over-estimation of D at intermediate densities since size effects can never be completely neglected; however, we believe the method proposed by Alder and Alley could lead to significant underestimation of D in the same density range.

Thus far we have only considered qualitative comparisons between current theories of diffusion in dense overlapping Lorentz gases and our MD simulations; however, we will now show that there are serious quantitative discrepancies in the results which these theories predict, particularly in the vicinity of the percolation threshold. In the anomalous diffusion regime the molecular dynamics power law exponent on the VACF tail is, on average, 1.59. The values predicted by the self-consistent repreated-ring kinetic theory of Maters and Keyes [33] and the memory function/mode-coupling theory of Gotze *et al.* [31, 32] are 4/3 and 3/2, respectively. The result obtained by Gotze *et al.* is in reasonable agreement with simulation but is still too low. In contrast, the more recent estimate of 1.69 provided by the random walk analysis of Machta and Moore [39] is too large.

In Figure 5 the simulation results for D^* (Table 2) reduced by the Boltzmann

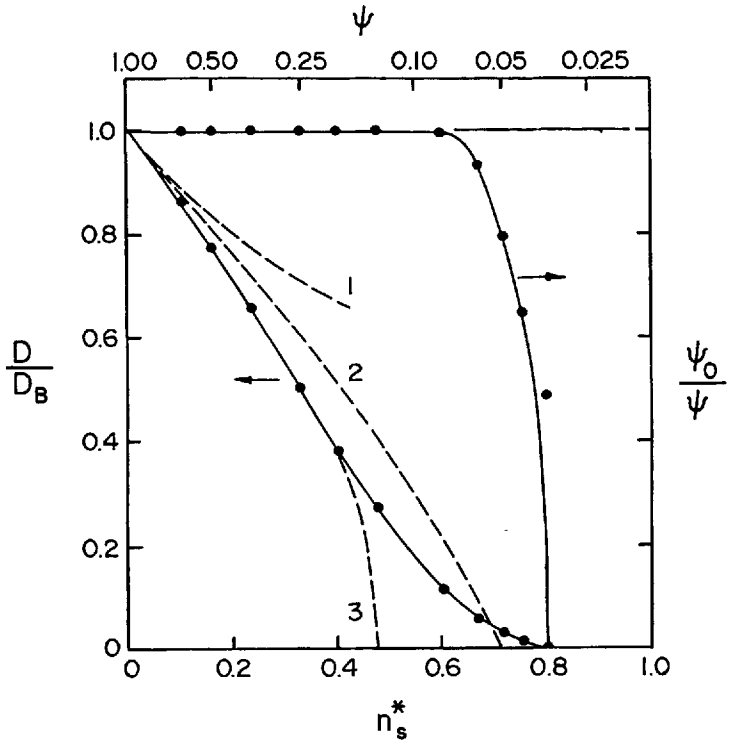

Figure 5 The diffusion coefficient reduced by its Boltzmann value (left ordinate axis) and the open porosity relative to the total porosity (right ordinate axis) as a function of reduced density (or porosity) for the random overlapping system. —— ● —— MD simulation; 1. kinetic theory for moderately dense systems (van Leeuwen and Weijland [28, 29]; 2. memory function/mode-coupling theory (Gotze *et al.* [31, 32]); 3. repeated ring kinetic theory (Masters and Keyes [33]).

diffusion coefficient are plotted as a function of n_s^* (or ψ). Also shown are the results predicted by (1) the kinetic theory of moderately dense Lorentz gases, which is exact to order n_s^{*2} [28, 29], (2) the theory proposed by Gotze *et al.* [31, 32], and (3) the theory proposed by Masters and Keyes [33].

Up to a density $n_s^* \sim 0.4$ it is seen that the repeated-ring kinetic theory of Masters and Keyes is in excellent agreement with the simulation results, whereas the memory function/mode couping approach of Gotze *et al.* leads to significant overprediction of D. The very favorable comparison with the theory of Masters and Keyes suggests that repeated ring events (i.e. repeated collisions of the gas particle with the same scattering center) dominate the diffusion process over this range of densities. The reasons for the poorer agreement of the theory of Gotze *et al.* is difficult to assess although it does appear to be due to the mode-coupling approximation which they employed. Masters and Keyes [33] have suggested that this approximation is similar to a ring (rather than a repeated ring) kinetic theory which leads to underestimation of the strength of the VACF tail (i.e. correlated events) and hence overestimation of D.

For densities greater than 0.4 the theory of Gotze *et al.* is better, although it still does not account for the correct density trends in D. The critical percolation density

n_{sc}^* which this theory predicts $(9/4\pi)$ is lower than the simulation result but is much better than the value $n_{sc}^* = 3/2\pi$ suggested by Masters and Keyes. In addition, the power law approach to n_{sc}^* (or ψ_c), which is known from percolation theory to be of the form

$$D \sim (\psi - \psi_c)^{\mu} \tag{12}$$

is better characterized by the memory function/mode coupling approximation with $\mu = 1$ than by repeated ring kinetic theory wherein $\mu = 1/2$.

Although the theory of Gotze *et al.* is better than that of Masters and Keyes near the percolation threshold, it may be seen from Figure 5 that both of these theories share one major deficiency, i.e., over most of the density range the trend in D/D_B is concave downwards. The simulation results on the other hand clearly show an inflexion point at a density $n_c^* \sim 0.4$ which, as noted above, is the density at which repeated-ring kinetic theory starts to deviate badly from the simulations. This is indicative of other correlated events coming into play, one possible example of which is the anticorrelation of the velocity of a gas particle as it enters and leaves a dead-end pore in the medium [39]. As the percolation threshold is approached, trapping, as indicated by the solid curve on the right hand side of Figure 5, will also start to dominate and the diffusing gas particle will be forced to move over the surface of increasingly larger nonpercolating clusters of solid spheres until, at the percolation threshold, the diffusion path length needed to traverse the medium diverges to infinity. There is currently no kinetic theory available that can adequately quantify this behaviour.

In addition to the kinetic or mode-coupling techniques discussed above one may also consider results predicted by the scaling rules of percolation theory. Bearing in mind that the molecular dynamics method (as well as the analyses involved in kinetic and mode-coupling theories) does not differentiate between trapped and untrapped states in the computation of the diffusion coefficient, than the scaling rule for $D(t^*)$ provided by Gefen *et al.* [40] (see also [41]) may be used to investigate some of the properties of the Lorentz gas near the percolation threshold. In the anomalous diffusion regime Gefen *et al.* have shown that

$$D^*(t^*) \sim 1/t^{*\delta} \tag{13}$$

where

$$\delta = \mu/(2\nu + \mu - \gamma) \tag{14}$$

μ is the power law exponent in equation (12), ν is a similar exponent for the correlation length

$$\xi \sim |\psi - \psi_c|^{-\nu} \tag{15}$$

and γ is the exponent for the percolation probability

$$P(\psi) \sim (\psi - \psi_c)^{\gamma} \tag{16}$$

$P(\psi)$ in the present case is equivalent to the ratio ψ_0/ψ. (Here we employ the notation γ for the power law exponent in Equation (16) since we have used β, which is the more common notation, in Equation (9). We also use the notation μ in equation (12) instead of t to avoid any confusion with time).

If we assume $\psi_c = 0.035$ then the results given in Table 2 which appear to conform

with Equations (12) and (16) are those for $\psi \leqslant 0.06$. The estimates obtained for μ and γ are 1.3 ± 0.2 and 0.3 ± 0.1 respectively. It has been suggested [42] that void space percolation in the random overlapping spheres model is in the same universality class as lattice percolation for which [43] $\mu = 1.90$ and $\gamma = 0.45$. The result we obtain for γ is not inconsistent with this hypothesis although our estimate of μ does appear to be low. This may be due to the limited amount of data which we have near the percolation threshold, as well as the sensitivity of μ and γ to the assumed value of ψ_c. A more direct test of the applicability of lattice percolation is to consider the value predicted for $\beta (= 1 + \delta)$ using Equation (14) and the lattice percolation value for $\nu = 0.88$ [43] as well as the values $\mu = 1.90$ and $\gamma = 0.45$. We find $\beta = 1.59$ in excellent agreement with the results given in Table 1.

2.2 *Results for Model (ii)*

We now turn to the results obtained for model (ii) (Figure 1(b)) which we believe is a better representation of high porosity ($\psi > 0.5$), consolidated porous media. In this case we consider only two values of ψ, 0.644 and 0.59, and we examine the properties of the dilute pore fluid over a range of fluid particle sizes, σ. The simulation studies for $\psi = 0.644$ are of sufficient extent to consider the behaviour of the VACF, the diffusion coefficient D^*, and the partition coefficient K in the vicinity of the percolation threshold. The runs conducted for $\psi = 0.59$ are, however, much shorter in length but serve an important purpose as will be shown below.

The parameters obtained from analysis of the long-time tails of the VACF in the connected system at the porosity $\psi = 0.644$ are given in Table 3. In this case we observe that the results for both α and β in the anomalous diffusion regime are significantly larger than in the random overlapping system. Furthermore, the range of conditions for anomalous diffusion is much broader in the connected system, corresponding to $0.9 \leqslant \sigma < 1.8$ for nonzero D^* (see Table 4), while for similar conditions in the random system this range may be shown to correspond to $0.8 \leqslant \sigma \lesssim 1.0$ using Equation (7).

The last run shown in Table 3 for $\sigma = 1.80$ is of interest in that it demonstrates how the tail of the VACF behaves above the percolation threshold. In this case the

Table 3 Parameters for the Long-Time Tails of the VACF. Connected Overlapping System ($\psi = 0.644$)

σ	Δt^{*a}	α^b	β^b
‡0.0	–	–	–
0.45	14–35	1.4(2)	2.19(6)
0.90	14–40	1.4(1)	1.93(3)
1.05	14–40	1.2(1)	1.88(3)
1.20	14–40	1.5(2)	1.95(5)
1.35	14–40	1.5(2)	1.96(4)
1.50	14–40	1.3(2)	1.93(3)
1.60	14–40	1.2(2)	1.92(5)
1.80	14–40	3.3(8)	2.23(6)
	40–120	0.8(1)	1.86(4)

[a] Δt^* is the time range, in simulated collison times, employed in the least-squares fit of the tail. The results for τ_c^* relative to the Boltzmann free time are given in Table 4.

[b] The second set of results for $\sigma = 1.80$ were obtained from a least-squares fit of $\ln D^*(t^*)$ to $\ln t^*$

‡ This run was of insufficient length to determine α and β. In each run the number of scatters employed and the number of configurations generated were 400 and 1000 respectivley. The total length of the trajectory in any given configuration was $16 \times 10^3 \tau_B^*$.

Table 4 Simulation Results for the Connected Overlapping System ($\psi = 0.644$)

σ	D^{*a}	P^b	K_T^c	R_p^{*d}	τ_c^*/τ_B^{*e}
0.0	0.952(2)	1.0	1.0	1.696	1.14(1)
0.45	0.356(2)	1.0	0.484(3)	1.043	1.51(3)
0.90	0.116(2)	0.991(3)	0.182(2)	0.813	2.11(7)
1.05	0.072(2)	0.94(1)	0.132(2)	0.743	2.3(2)
1.20	0.042(2)	0.75(2)	0.088(2)	0.691	2.5(2)
1.35	‡0.024(2)	0.48(2)	0.054(3)	0.627	2.6(2)
1.50	‡0.009(2)	0.25(3)	0.036(2)	0.546	2.5(2)
1.60	‡0.006(1)	0.16(2)	0.027(2)	0.494	2.5(2)
1.80	‡0	(0.039)	0.014(1)	0.388	2.2(2)

[a] As in Table 2.
[b] P is the percolation probability which is synonymous with $\psi_0 \cdot \psi$ in Table 1. P is equivalent to $\psi_0 \cdot \psi$ if the moving particle is contracted to a point and the scattering centers are increased in size to $\sigma_s + \sigma$. The nonzero value of P for $\sigma = 1.80$ is indicative of size effects.
[c] K_T is the total partition coefficient, trapping regions included, determined from 10^3 Monte Carlo trial insertions in each of the configurations generated for the connected system. These results represent less than half of the runs conducted to obtain the curve shown in Figure 7(b).
[d] R_p^* is the average half-length of the free trajectories or the equivalent mean pore radius if the moving particle is treated as a point and the scatterers are expanded to $\sigma_s + \sigma$.
[e] τ_c^* is the mean free time determined from the simulations and τ_B^* is the Boltzmann mean free time at the corresponding value of n_s^* and σ. All time scales in Table 3 and Figure 6 are in units of τ_c^*.
‡ These diffusion coefficients were obtained by extrapolating the long-time tails in Table 3. The run for $\sigma = 1.80$ is above the percolation threshold.

intermediate-time tail has a power law exponent well above the average value 1.92 for anomalous diffusion; however, the long-time result between $t^* = 40$ and $t^* = 120$ has a value that is more appropriate to conditions at the percolation point. It is expected that at higher values of σ the power law on the intermediate-time tail will

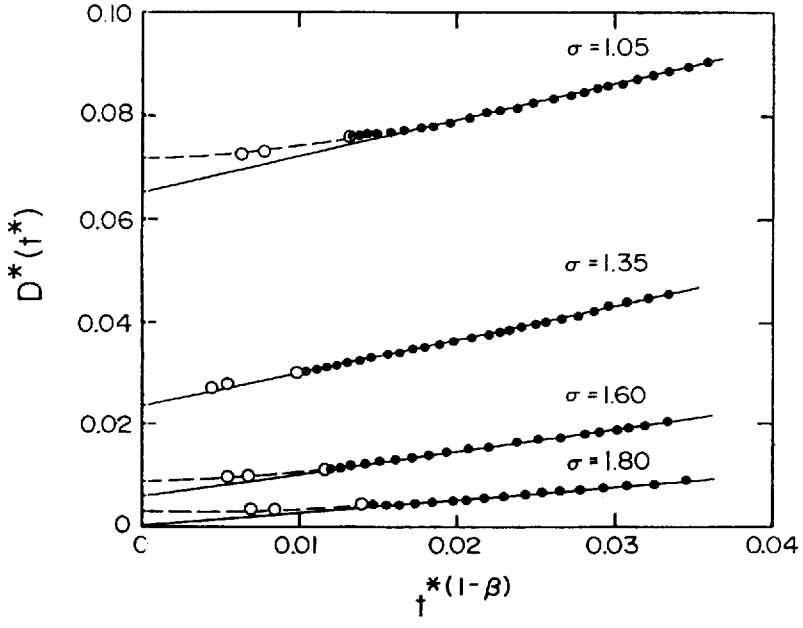

Figure 6 The time dependent diffusion coefficient for several fluid particle sizes in the connected overlapping system ($\psi = 0.644$). All symbols are as in Figure 3. The power law exponents are: $\beta = 1.88$ ($\sigma = 1.05$); 1.96 ($\sigma = 1.35$); 1.92 ($\sigma = 1.60$); 1.86 ($\sigma = 1.80$).

continue to increase and the transition to a value ~ 1.9 will occur at later times. The full line for $\sigma = 1.80$ in Figure 6 corresponds to Equation (11) with $\alpha = 0.8$, $\beta = 1.86$ and an infinite-time diffusion coefficient equal to zero. For times $t^* > 120$ the simulation results deviate from this line due to size-effects which have a much greater influence here than for the random overlapping structure. For $\sigma \leqslant 1.35$ density fluctuations are negligible and for reasons given earlier, the long-time results shown in Figure 6 for $\sigma = 1.05$ are believed to be largely due to an hydrodynamic tail.

The results obtained for D^* by extrapolating the simulation data to infinite times are given in Table 4. Also shown in this table are the percolation probabilities P, the (total) partition coefficients K_T, the average half-length of the free trajactories, R_p^*, reduced by σ_s, and the magnitude of the simulated mean free time τ_c^* relative to the Boltzmann value (Equation (5)). The latter results are typically a factory of two larger than τ_B^* in the anomalous diffusion regime and this simply reflects the fact that the generation of a macroscopically connected cluster of solid spheres using the procedure discussed in the Appendix is equivalent to moving small isolated clusters in the random overlapping structure into direct contact with the largest cluster in the system. (A simple example of induced solid phase continuity is schematically illustrated in Figures 1(a) and 1(b) where the isolated sphere 1 in the random model is moved to form a bridge in the connected system). While this only marginally increases the mean free time, as well as R_p^*, for the case $\sigma = 0$, we see that solid phase connectivity has a dramatic effect on the percolation properties of the overlapping spheres model at high porosities. Furthermore, in comparing the result for R_p^* at the percolation threshold with the corresponding value in Table 2, we observe that the average size of the cavities within which an equivalent point particle is trapped is approximately twice as large in the connected system. This has a direct bearing on the interpretation of the topology of the pore space which will be considered in more detail below.

In Figure 7(a) we plot the diffusion coefficient in the connected system reduced by its value for $\sigma = 0$ as a function of σ. Also shown are the equivalent results for the random structure which are replotted from Figure 3 using Equation (7) with ψ fixed at 0.644. This figure further demonstrates the influence of connectivity of the solid phase and illustrates clearly the large shift in the position of the percolation threshold referred to earlier. In this case the transition occurs in the range $1.6 < \sigma < 1.8$ and is indicated approximately at $\sigma \sim 1.75$ in Figure 7(b) where we plot the partition coefficients for both the random (Equation (8)) and connected systems as a function of σ.

In Figure 7(b) we indicate one of the reasons we chose to conduct simulations at a porosity $\psi = 0.644$. A rarified gas has a one-to-one correspondence with infinitely dilute solutions of macromolecules and the open squares in Figure 7(b) are the experimental partition coefficients reported by van Kreveld and van den Hoed [44] for polystrene spheres distributed between a bulk liquid phase and the pores of a silica based material Porasil C. This material is believed to have a solid structure similar to the sphere models under consideration here and in fact van Kreveld and van den Hoed found their experimental results to be in good agreement with the random overlapping spheres model. The manner in which we have plotted these results however raises a question concerning the validity of one of the assumptions van Kreveld and van den Hoed made in correlating their data. In their analysis they assumed that the equivalent radii of their polystyrene spheres were equal to $0.886\ R_g$, where R_g is the root mean square radius of gyration of the polymer molecule. A more common method used to correlate data for macromolecular partition coefficients however is by way of

the radius of gyration itself [45–47]. In Figure 7(b) we have plotted the experimental data as a function of $\lambda = R_g/R_P(= \sigma/R_P^*(\sigma = 0))$ for the connected system using the original values of R_g provided by van Kreveld and van den Hoed as well as their value $R_P = 244$Å for the hydraulic mean pore radius $2\psi/S$ (S = BET surface area of the solid).

The experimental data of van Kreveld and van den Hoed are seen to scatter around the simulation results for the connected system with the largest deviations occurring above $\lambda \sim 0.5$. This scatter may reflect the influence of a number of factors, one of which could be polydispersity of the inclusions forming the solid phase of the Porasil

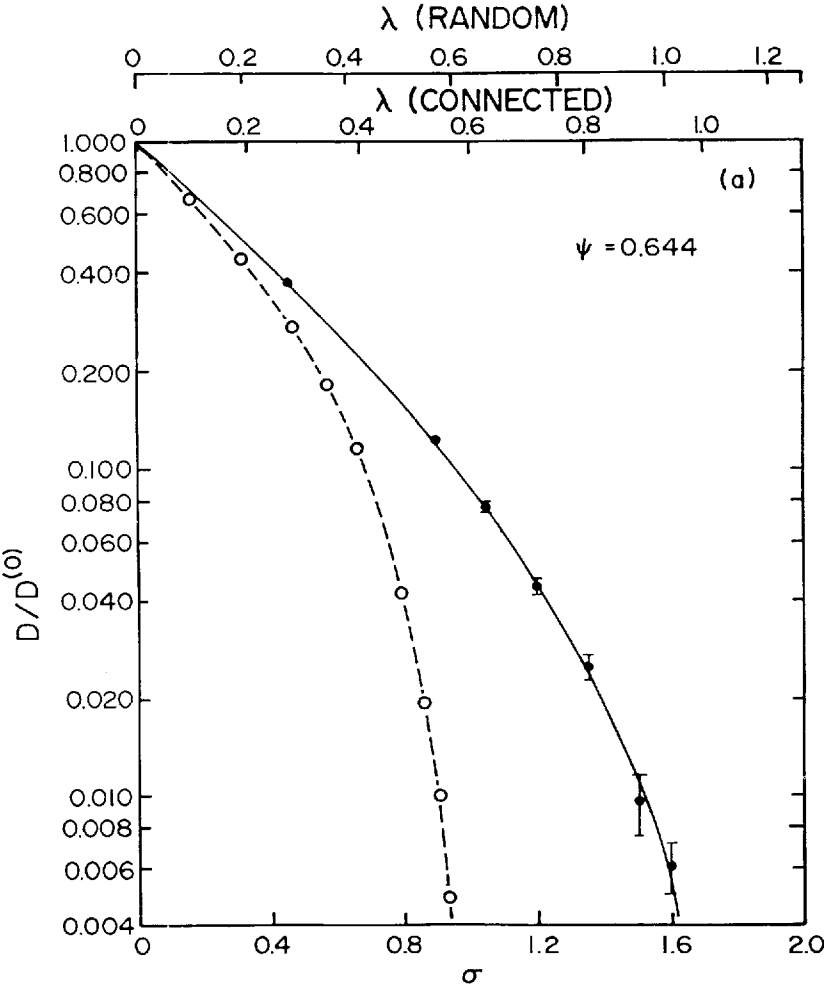

Figure 7 (a) The diffusion coefficient reduced by its value for $\sigma = 0$ as a function of fluid particle size (lower abscissa) or particle reduced size $\lambda = \sigma/R_P$ ($\sigma = 0$) (upper abscissa) in overlapping systems ($\psi = 0.644$) ·····○– – – random overlapping system; ——●—— connected overlapping system.

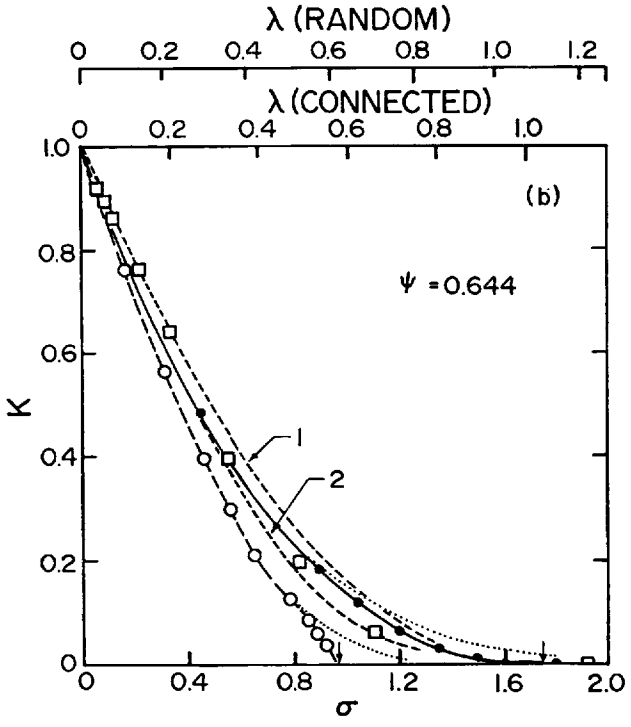

Figure 7 (b) The partition coefficient as a function of fluid particle size for the systems in (a). – – – o – – – and ——— ● ——— simulation results for the random and connected structures respectively (the dotted lines are the continuation of these results with trapping regions included); □ experimental data of van Kreveld and van den Hoed [44] for partitioning of polystyrene in Porasil C; 1. – – – theoretical result for partitioning of a hard-sphere fluid in cylindrical pores (Equation (18)); 2 – – – theoretical results [48, 49] for partitioning of random coiling polymer molecules in cylindrical pores (Equation (17)).

medium. Polydispersity in the random overlapping spheres model leads to smaller partition coefficients [11] since random placement of a small, unconnected sphere near a larger particle can significantly reduce the pore volume available to the center of the macromolecular solute. In the case of connected structures however we believe the opposite will be true, since one can imagine the reduction of a number of solid spheres to many smaller particles which are connectedly distributed throughout the medium, thereby opening the pore space to the solute. This may explain the positive deviation of the experimental data at small values of λ. Another explanation needs to be sought to account for the discrepancies observed above $\lambda \sim 0.5$ and, in particular, for the experimental point shown above the percolation threshold. One possible reason for this is given as follows. Polystyrene is a random coiling macromolecule and the statistics associated with coil configurations should be taken into consideration when comparing experimental K-values with theory. The only theory we know of which considers the influence of polymer chain configurations on the partition coefficient is that of Cassassa [48] and Casassa and Tagami [49]. For example, for cylindrical pores they find

$$K = 4 \sum_{m=1}^{\infty} \frac{1}{\beta_m^2} \exp(-\beta_m^2 \lambda^2) \tag{17}$$

where β_m are the roots of $J_0(\beta_m) = 0$. Equation (17) is plotted in Figure 7(b) as a function of λ for the connected system. The agreement with the data of van Kreveld and van den Hoed is surprisingly good even though the pores of the connected overlapping structure are not really cylindrical in shape. However we also observe that the simple expression for partitioning of dilute hard-sphere fluids in cylindrical pores

$$K = (1 - \lambda)^2 \tag{18}$$

is also in fair agreement with the simulation data. Our reasoning therefore, is that the connected overlapping system is a better representation of Porasil C than the random overlapping system and that the deviation of the data of van Kreveld and van den Hoed from the hard-sphere simulation results may be primarily due to polydispersity of the silica microspheres and coil configurations within the polystyrene macromolecules. On a more general level, the reasonable agreement between Equation (18) and the simulation results for model (ii) at $\psi = 0.644$ suggests that the connected spheres structure may be a valid model for a wider range of amorphous porous media particularly in view of the frequent use of the cylindrical pore model as a description of the void space in such systems. In this regard it is of particular interest to note that in the range of porosities where the random overlapping spheres model is naturally bicontinuous ($\psi \lesssim 0.5$), the expression for K_T given in Equation (8) is also in good agreement with Equation (18) for $\lambda < 0.5$.

The diffusion results shown in Figure 7(a) are, of course, only applicable to gases or, more specifically, nonadsorbing gases. It has already been noted [10] that there are few data available for comparison with size-exclusion results of the type shown in Figure 7(a) due to the predominant influence of adsorption and surface diffusion in micropores. However, some data do exist and here we will consider one particular case which we feel is most appropriate to the spheres models analyzed in this paper.

In two independent studies, Schneider and Smith [50] and Gangwal *et al.* [51] used pulse chromatography to determine the Knudsen diffusivity of simple hydrocarbon molecules in a silica gel with the same pore characteristics ($\psi = 0.49$, $R_P = 11$ Å). For ethane diffusion at moderately high temperatures Schneider and Smith estimated a "tortuosity" factor $q = 3.35$ while Gangwal *et al.* obtained the value $q = 2.4$ for diffusion of methane. To estimate the corresponding values of q for the overlapping spheres model we note the following.

The porosity of the silica gel, $\psi = 0.49$, was determined by helium expansion pycnometry with the implicit assumption that the helium atom is a point particle, i.e.,

Table 5 Simulation Results for the Connected Overlapping System ($\psi = 0.59$)

σ	D^{*a}	K_T^a	R_P^{*a}	τ_t^*/τ_B^{*a}
0.0	0.714(6)	1.0	1.376	1.09(3)
0.114	0.551(5)	0.83(1)	1.168	1.15(3)
0.20	0.442(5)	0.706(9)	1.034	1.19(2)
0.25	0.388(4)	0.636(5)	0.981	1.23(3)

[a] As in Table 4. The percolation probability P was equal to 1.0 in each run. The number of scatterers employed and the number of configurations generated in each case was 400 and 500 respectivley and the individual trajectories for each configuration were $2 \times 10^3 \tau_B^*$ in length.

its partition coefficient K is equal to 1.0. The helium atom, however, has finite size and its hard-sphere radius is given by Chapman and Cowling [52] as 1.09 Å. We can use Equations (2) and (7) and the equation [44]

$$\sigma_s = -(3/2)\, R_P \ln(\psi(\sigma = 0)) \tag{19}$$

to show that the true porosity ψ of the silica gel in the random spheres approximation is 0.59 and $R_P = 13$ Å (we assume the BET surface area S in the equation $R_P = 2\psi/S$ is unaffected). We therefore find that the value of K for helium is 0.83 and the estimated value of λ in this case is 0.082. If we assume that this value of λ also applies for the connected system then, in view of the weak dependence of $K(\lambda)$ on ψ as indicated by the agreement between Equation (18) and the K-values for connected structures, we may infer from Figure 7(b) that $\psi = 0.59$ for model (ii) as well.

Four simulation runs of comparatively short duration were conducted for the connected overlapping spheres model at a porosity $\psi = 0.59$ and the results obtained are presented in Table 5. The nonzero reduced radii shown in this table correspond to helium ($\sigma = 0.114$ (1.09 Å)), methane ($\sigma = 0.20$ (1.9 Å)), and ethane ($\sigma = 0.25$ (2.4 Å)). The hard-sphere radii for methane and ethane were estimated at the temperature of the experiments and the reduced radii σ were determined using $\sigma = \lambda R_P^*$ ($\sigma = 0$) where the values of λ employed in this expression are based on $R_P = 13$ Å.

A comparison between the results shown in Table 5 and the experimental data of Schneider and Smith and Gangwal *et al.* may be made by noting that the equation employed in references [50] and [51] to determine the "tortuosity" factor was

$$q = \psi\,(2/3\, v R_P)/D_P \tag{20}$$

where D_P is the experimental pore diffusivity, $\psi = 0.49$ and $R_P = 11$ Å. In addition to the corrections to $\psi (= \psi K_{He})$ and R_P, we must also take into consideration that the definition for D_P employed by Schneider and Smith and Gangwal *et al*, is, in our notation, $\psi K_i D$ where K_i is the partition coefficient of species i (see Equations (1) and (2)). Furthermore, another factor that needs to be included is the influence of diffuse reflection which is generally accepted as being the primary mode of particle scattering at solid surfaces. For elastic diffuse scattering in dilute isotropic sphere assemblies, Derjaguin [53] and Mason and Chapman [54] have shown that a factor 9/13† needs to be introduced into the theoretical expression for the diffusion coefficient (see also [55]). There is reason to believe [57, 58] that the factor 9/13 is applicable at all densities n_s^* and/or diffusing particles sizes and we assume this to be the case here.

With the above modifications, Equation (20) can be written in terms of the dimensionless quantities provided in Table 5 as

$$q = (26/27)\,(K_{He}^2/K_i)\,(R_P^*(\sigma = 0)/D^*) \tag{21}$$

The theoretical results for the connected overlapping system are found to be $q = 2.93$ (methane) and 3.70 (ethane). Similarly, by using Equations (7) and (8) and interpolating the data given in Table 2 we find that for the random overlapping model $q = 3.16$ (methane) and 4.15 (ethane). The results for the connected system are in better agreement with experiment, particularly for the larger diffusing species where we expect the influence of connectivity to be more pronounced.

†For thermal diffuse scattering [56] this factor is $1/(1 + \pi/8)$ which differs by only a few precent.

To conclude this section we consider one other aspect of the void-space structure of the high porosity connected system which is inferred by the scaling rule of Gefen *et al.* [40]. In the anomalous diffusion regime we have already noted that the average value of the exponent β in the long-time tail of the VACF for the connected system at $\psi = 0.644$ is 1.92, i.e., δ in Equation (14) is 0.92. If we assume $\delta \sim 1$ then using Equation (14) we find $2\nu \sim \gamma$ or, since the power law exponent in Equation (16) is generally less than or equal to 1.0, $\nu \leqslant 0.5$. Low values of the correlation length exponent ν typically arise in the percolation theory of randomly branched structures [59]. This suggests that the pore space of the high porosity connected system is tree-like and, from our earlier comment regarding the size of R_p^* at the percolation threshold and also the magnitude of σ in this range, it would seem that much of the pore volume resides in large cavities similar to those appearing in a number of models which are frequently employed to explain the characteristics of hysteresis loops in adsorption/desorption isotherms (see for example [60]). We can also consider a more accurate evaluation of ν by estimating both μ in Equation (12) and γ in Equation (16) from a least-squares fit of the data given in Table 4 near the percolation threshold. In this case the total porosity in both these equations is replaced by ψK_1 where $\psi = 0.644$ and K_1 is the overall partition coefficient. By fitting the four points between $1.05 \leqslant \sigma \leqslant 1.50$ (the scatter in the values at $\sigma = 1.60$ appears to be too large) we find $K_c = 0.016 \pm 0.004$ (i.e., $\sigma_c \sim 1.75$), $\mu = 1.1 \pm 0.1$, and $\gamma = 0.75 \pm 0.1$. With $\delta = 0.92$ the value of ν is found to be 0.42 ± 0.05. We also observe that the value of γ is more consistent with percolation on a branched structure than with site percolation on a lattice [43]. The value of μ however is quite low and we can offer no explanation for this at present. Although more extensive computations near the percolation threshold may be needed to verify this result, it is clear that outside the range of porosities in which the random overlapping spheres model is naturally connected, the exponents in Equations (12)–(16) undergo a radical change when connectivity is enforced on the system. For porosities higher than those investigated here we anticipate that the exponent β on the longtime tail of the VACF in the connected system will be larger than 1.92 with corresponding changes in the values of μ, γ and ν.

3 NONOVERLAPPING SYSTEMS

The appropriate collision time for the moving particle in nonoverlapping systems is the Enskog mean free time which is given by

$$\tau_c(v/\sigma_s) = \tau_E^* = 1/(\pi n_s^* g(\sigma)(1 + \sigma)^2) \tag{22}$$

$g(\sigma)$ is the contact pair correlation function for the moving particle and one of the scatterers and for nonzero σ is given approximately by the Carnahan-Starling Equation [61] as

$$g(\sigma) = \frac{1}{\psi}\left[1 + 3\left(\frac{\sigma}{1+\sigma}\right)\left(\frac{1-\psi}{\psi}\right) + 2\left(\frac{\sigma}{1+\sigma}\right)^2\left(\frac{1-\psi}{\psi}\right)^2\right] \tag{23}$$

where ψ is the tota' porosity of the medium

$$\psi = 1 - (4/3)\pi n_s^*$$

Equation (22) is exact for random nonoverlapping systems. However, we will show

that at low porosity (high density) errors incurred by the approximate expression for $g(\sigma)$ in Equation (23) can lead to significant deviations in the predicted mean free times away from the simulation results. We will also show that Equation (22) with Equation (23) underestimates τ_c^* for connected structures at moderate to high porosities.

The framework for the presentation of the results for diffusion and partitioning will be similar to that for the overlapping systems although in the present case there are fewer theoretical results available with which comparison can be made. The diffusion coefficient predicted by Enskog

$$D_E^* = 1/(3\pi n_s^* g(\sigma)(1 + \sigma)^2) \tag{24}$$

will serve as a basis for the discussion of the MD simulation data and the partition coefficient obtained from the definition of the chemical potential in the Carnahan-Starling approximation [61]

$$\begin{aligned} \ln K = {} & \sigma^2(2\sigma - 3)\ln\psi - \sigma(3 + 6\sigma + \sigma^2)((1 - \psi)/\psi) \\ & - 3\sigma^2(1 + \sigma)((1 - \psi)/\psi)^2 - \sigma^3(2 - 3\psi - \psi^2)((1 - \psi)/\psi^3) \end{aligned} \tag{25}$$

will play a similar role in the discussion of the Monte Carlo results for partitioning. Other expressions for K are available, for example from scaled particle theory [10, 11]; however, Equation (25) is employed here due to its higher accuracy.

3.1 Results for Model (iii)

To investigate the properties of nonoverlapping systems we have conducted simulations at two porosities and determined both D^* and K over a range of diffusing particle sizes. Our first studies involve simulations at a porosity $\psi = 0.367$ which is within 1% of the porosity of the most dense random packing known for nonoverlapping equal-sized spheres [17–19]. The random close-packed (RCP) structure has received considerable attention as a model for amorphous metallic glasses (see for example [62]) and in this respect the results to be presented below may be considered to be representative of impurity transport in such systems.

In Figure 8 we plot the VACF's obtained for two sizes of the particle moving within the RCP structure. The insets illustrate the characteristic long-time behaviour of the VACF tails from which the parameter values given in Table 6 were obtained. For small particle sizes the power law tail is hydrodynamic within computational error and the dashed line in the inset of Figure 8(a) corresponds to the theoretical result obtained by Ernst *et al.* [34, 35] for $C(t^*)$ at long times

$$C(t^*) = -\frac{(3\pi)^{1.5} n_s^{*2}}{16(\psi t^*)^{2.5}} \left(\frac{S_0(n_s^*)}{n_s^*}\right) \left\{\frac{d \ln D^*}{d \ln n_s^*} - \left(\frac{1 - \psi}{\psi}\right)\right\}^2 \left(\frac{D_B}{D}\right)^{1/2} \tag{26}$$

The quantity $S_0(n_s^*)$ in this equation is the eqilibrium density fluctuation and is directly related to the isothermal compressibility of the system. For the RCP structure we have used the high density equation-of-state data provided by Alder and Wainwright [63] to find $S_0(n_s^*)/n_s^* = 0.008$ (this is much smaller than the corresponding value of 1.0 for the overlapping system and, as we will see, the significantly reduced effect of density fluctuations has important consequences in our simulation results). The derivative in equation (26) was calculated assuming $D^* \sim D_E^*$ which is a very

Table 6 Parameters for the Long-Time Tails of the VACF. Nonoverlapping System ($\psi = 0.367$)

σ	Δt^{*a}	α^b	β^b
0.0	10–18	0.29(6)	2.4(1)
		0.34(6)	2.5
0.05	10–22	0.84(8)	2.47(3)
		0.91(7)	2.5
0.10	18–55	0.7(2)	2.0(1)
0.15	18–55	0.50(5)	1.63(3)
0.175	18–55	0.42(3)	1.52(2)
0.20	18–55	0.33(3)	1.42(2)
0.225	18–55	0.39(2)	1.46(2)
0.25	18–55	0.36(2)	1.44(2)

[a] As in Table 3. The results for τ_ζ^* relative to the Enskog mean free time estimated using the Carnahan-Starling equation are given in Table 7.

[b] The second set of results for $\sigma = 0.0$ and 0.05 were obtained from a fit to $t^{*-2.5}$. In each run the number of scatterers employed and the number of configurations generated were 200 and 1500 respectively. The length of the trajectory in each individual configuration was $16 \times 10^3 \tau_\zeta^*$(C-S) where τ_ζ^*(C-S) is defined in Table 7.

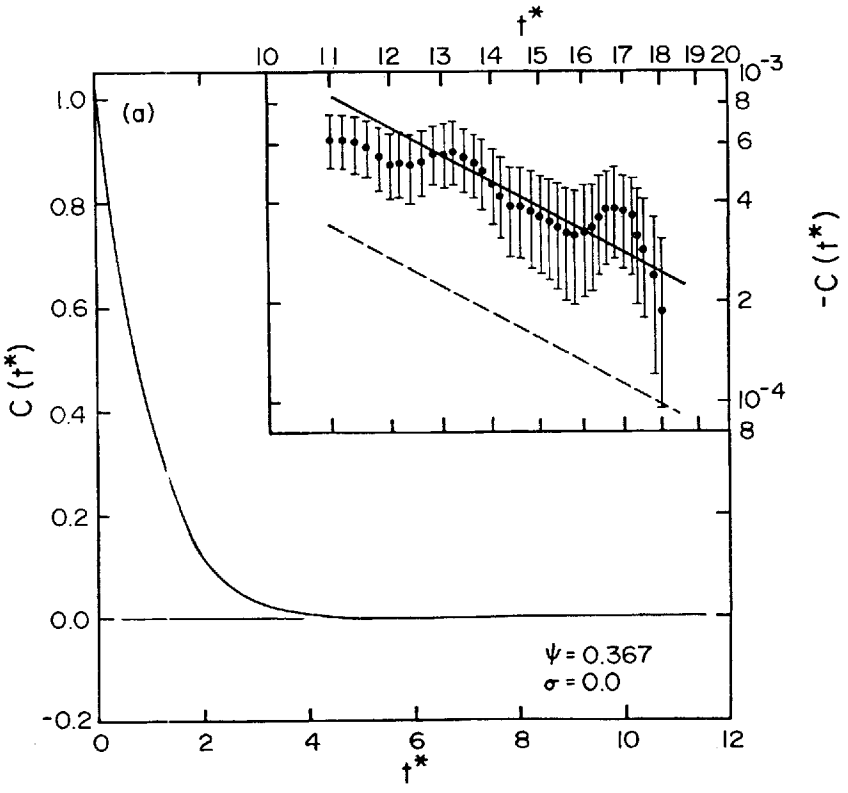

Figure 8 (a) Normalized velocity autocorrelation function for the random close-packed nonoverlapping system ($\psi = 0.367$, $\sigma = 0$). The inset shows the long-time tail: ● MD simulation; —— fit to a $t^{*-2.5}$ power law decay; – – – – mode coupling theory of Ernst *et al.* [34, 35].

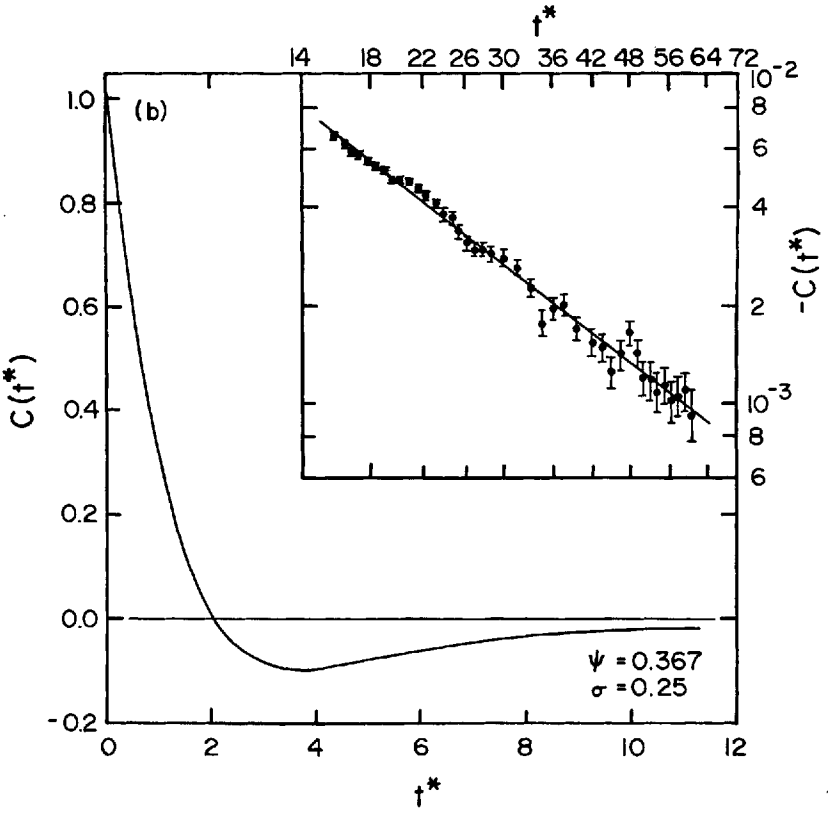

Figure 8 (b) VACF for $\sigma = 0.25$. The long-time tail is shown in the inset: ● MD simulation; —— least squares fit to a $t^{*-\beta}$ power law decay ($\beta = 1.44$).

good approximation for $\sigma = 0$ at both porosities investigated here. Using this approximation and the result for $S_0(n_s^*)$ the estimated value of α in Equation (9) is found to be 0.14. This result is much lower than the simulated value 0.34 with a deviation comparable to that for the random overlapping system at the same value of ψ.

As the particle size σ is increased the power law parameters given in Table 6 follow trends similar to those observed earlier for the overlapping systems. Both α and β decrease most rapidly as the value $\sigma = 0.15$ is approached and this is directly related to the statistical geometry of the tetrahedra of scatterers which predominate in the RCP structure [17–19]. The triangular faces of the highest density tetrahedra have holes which can accommodate a fluid particle of size $\sigma \leqslant 0.155$ and above this value of σ we can expect a radical change in diffusion path characteristics. This is clearly evident in Table 6 with anomalous diffusion setting in at $\sigma \sim 0.2$. In this case we also observe an average value for $\beta = 1.44$ which is significantly lower than the results obtained in the overlapping systems. In light of the results for β obtained by Gotze *et al.* [32] and Masters and Keyes [33] for the random overlapping system ($\beta = 3/2$ and $4/3$ respectively) it is tempting to suggest that the low value of β found here may reflect

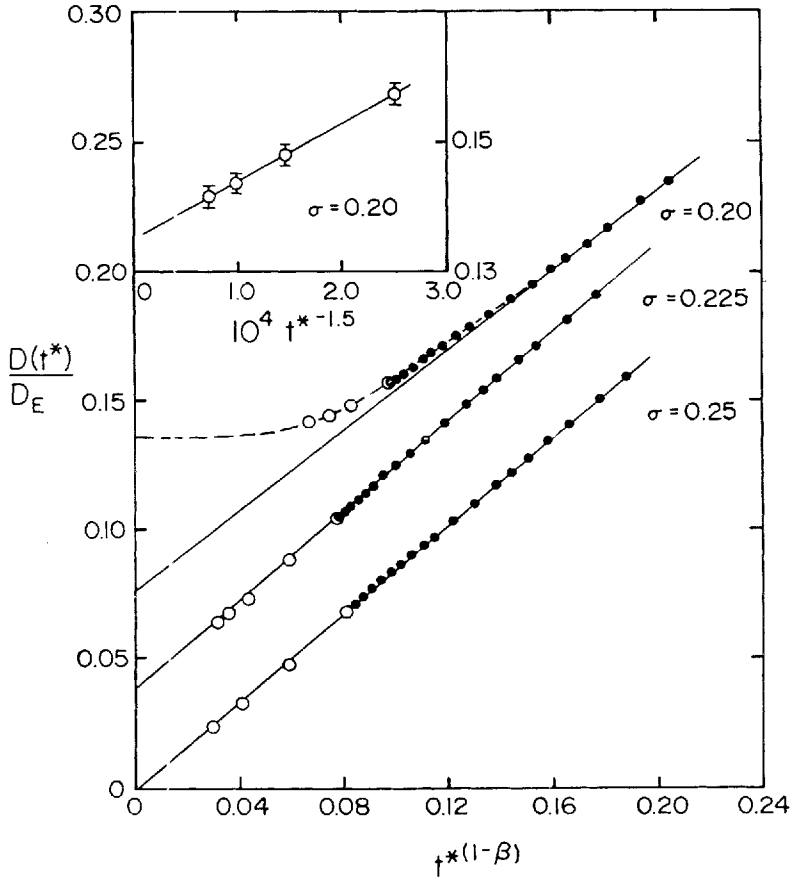

Figure 9 The time dependent diffusion coefficient in the random close packed nonoverlapping structure ($\psi = 0.367$) for several fluid particle sizes near the percolation threshold. D_E is the Enskog diffusion coefficient and the inset illustrates the long-time ($250 < t^* < 575$) hydrodynamic power law for $\sigma = 0.20$. The remaining symbols are as in Figure 3. The power law exponents for the straight lines shown in the main figure are: $\beta = 1.42$ ($\sigma = 0.20$); 1.46 ($\sigma = 0.225$); 1.44 ($\sigma = 0.25$).

the importance of ring events in the RCP structure. A direct analytical investigation of this possibility, however, does not appear to be feasible at present.

The time-dependent diffusion coefficients for the three largest particle sizes are shown in Figure 9. D_E in the ordinate of this figure is the dimensional form of Equation (24) with $g(\sigma)$ determined from the simulation results for τ_c^* (Table 7) rather than the Carnahan-Starling equation. It is noteworthy that even though the number of scatterers employed is comparatively small ($N_s = 200$) the influence of density fluctuations near the percolation threshold is essentially nonexistent. For $\sigma = 0.225$ and 0.25 direct extrapolation of Equation (11) with the parameters in Table 6 is indicated to determine the infinite-time diffusion coefficients given in Table 7 and the percolation threshold is seen to occur at the value $\sigma = 0.25$.

The results for $\sigma = 0.20$ shown in Figure 9 also provide a resolution to one of the

Table 7 Simulation Results for the Random Close-Packed Nonoverlapping System ($\psi = 0.367$)

σ	D^{*a}	P^b	K_T^c	R^{*c}_P	$\tau_c^*/\tau_E^*(C\text{-}S)^d$
0.0	0.2422(8)	1.0	1.0	0.406	1.000(3)
0.05	0.1638(6)	1.0	0.79(2)	0.326	1.125(4)
0.10	0.1040(2)	1.0	0.56(1)	0.265	1.218(5)
0.15	0.0496(2)	1.0	0.37(1)	0.219	1.276(6)
0.175	0.0294(1)	1.000(2)	0.29(1)	0.202	1.33(1)
0.20	0.01657(3)	1.00(1)	0.22(1)	0.187	1.39(2)
0.225	‡ 0.0043(2)	0.71(5)	0.170(8)	0.173	1.41(3)
0.25	‡ −0.00002(5)	(0.16)	0.127(7)	0.158	1.39(5)

[a] As in Table 2.
[b] As in Table 4. We believe the existence of a nonzero value for P at $\sigma = 0.25$ is indicative of size effects.
[c] As in Table 4.
[d] τ_c^* is the mean free time determined from the simulations and $\tau_E^*(C\text{-}S)$ is the Enskog free time estimated using the Carnahan-Starling equation for the contact pair correlation function. All time scales in Table 6 and Figures 8 and 9 are in units of τ_c^*.
‡ These diffusion coefficients were obtained by extrapolating the long-time tails given in Table 6.

issues raised earlier in the discussion of the random overlapping system, namely the existence or nonexistence of hydrodynamic tails at very long times. The four open circles shown in this case correspond to the time-dependent diffusion coefficients obtained from the slope of the mean-square displacement in the time range $250 \leqslant t^* \leqslant 575$. The upper limit $t^* = 575$ was found to be the average time required for the diffusing particle to travel a distance equivalent $0.48\,L^*$ where L^* is the side length of the fundamental cell in units of σ_s. Noticeable deviations from the straight line obtained by extrapolating the intermediate-time tail with $\beta = 1.42$ are also seen to occur as early as $t^* \sim 100$ which corresponds to a root mean-square displacement of $0.24\,L^*$ ($\sim 2.6\,\sigma_s$). We feel that these distances are short enough to disregard any effects which may arise due to the periodic boundary conditions and that the long-time results shown in Figure 9 are therefore solely due to an hydrodynamic tail. To illustrate this, the inset in Figure 9 indicates the accuracy with which the hydrodynamic power law can correlate the four long-time points shown in the main figure.

The equlibrium and dynamical properties determined for the RCP Lorentz gas are presented in Table 7. The Enskog mean free times employed in computing the results given in the last column of this table were calculated using Equations (22) and (23) and the differences observed are due to overestimation of $g(\sigma)$ in the Carnahan-Starling approximation. Equation (23) is exact only for point particles ($\sigma = 0$) at this high a density. We also note the non-zero value for the percolation probability P at the percolation threshold, illustrating the influence of finite system size even though density fluctuations have a negligible effect on $D^*(t^*)$ for the time range shown in Figure 9.

In Figure 10(a) we plot the diffusion coefficient relative to the point particle Enskog value $D_E^{(0)}/v\sigma_s = 4\psi/9(1\text{-}\psi)$ as a function of diffusing particle size. Also shown in this Figure are the results predicted by Enskog's equation with $g(\sigma)$ corrected for particle size effects using the simulated mean free times given in Table 7. Enskog's theory is quite accurate for $\sigma = 0$ which is not surprising in view of the near exponential behaviour of the VACF in this case (Figure 8(a)). However, as σ approaches the percolation threshold, dynamical correlations arising from backscattering and trapping (as indicated by the negative region in the VACF shown in Figure 8(b)) dominate the diffusion process and Equation (24) is understandably poor under these conditions.

The result for D^* in the case $\sigma = 0$ is of interest in light of the theoretical

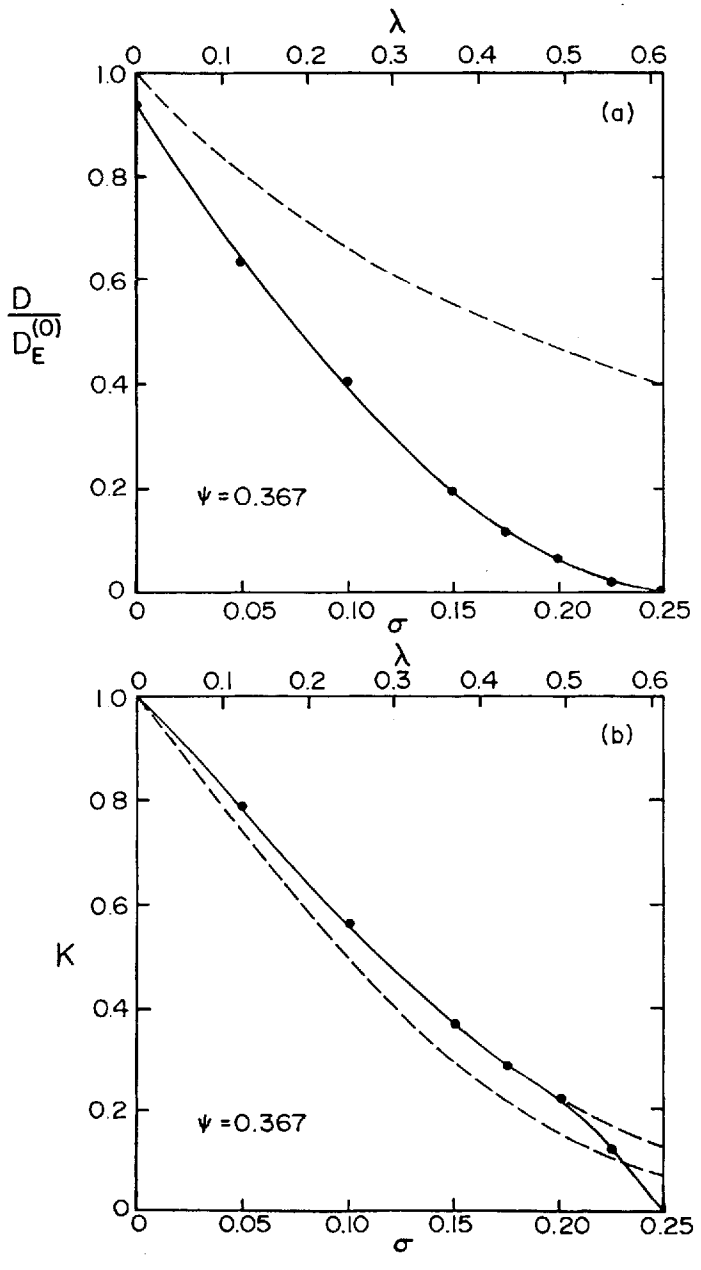

Figure 10 Diffusion and partitioning in the random close packed nonoverlapping system ($\psi = 0.367$). (a) The diffusion coefficient reduced by its Enskog value for $\sigma = 0$ as a function of σ (lower abscissa) or λ (upper abscissa) —— ● —— MD simulation; - - - - Enskog equation.
(b) The partition coefficient as a function of fluid particle size for the system in (a). ● —— simulation (the dashed line continuation represents the simulation results with trapping regions included); - - - - predicted by the Carnahan-Starling equation (Equation (25)).

calculations of van Leeuwen and Weijland [28, 29] and Masters and Keyes [64]. At low to moderate densities the exact expression for D^* with $\sigma = 0$ is

$$D^* = [3\pi n_s^*(1 + (4/3)\pi n_s^* + 1.234 n_s^* + 0(n_s^{*2} \ln n_s^*) + \text{----})]^{-1} \quad (27)$$

The term $(4/3)\pi n_s^*$ in the denominator of this equation is the first density correction predicted by Enskog through the contact pair correlation function $g(\sigma = 0)$. The second term of order n_s^* is the correction arising from dynamical correlations and is seen to represent a significant contribution to the density dependence of the diffusion coefficient. In contrast, we find Enskog's equation alone, with possible minor corrections due to dynamical effects, to be adequate at the high density corresponding to $\psi = 0.367$ (and also $\psi = 0.644$ as will be seen below) and this suggests at least a partial cancellation of the contribution $1.234 n_s^*$ by higher order terms in the expansion in Equation (27). This observation raises a question concerning the applicability of the ad hoc formulation of D^* recently proposed by James and Evans [27]. In their studies of the two-dimensional nonoverlapping Lorentz gas James and Evans found that, by simply replacing the inverse density expansion for D^* by a multiple of $g(\sigma = 0)$ and the leading dynamical corrections, very good agreement with their simulation results could be obtained. If we apply this procedure to the three-dimensional case, noting that the logarithmic term in Equation (27) is negligible, we find for $\sigma = 0$

$$D/D_E = 1/(1 + 1.234 n_s^*)$$

For $\psi = 0.367$ this predicts $D/D_E = 0.84$ which is significantly lower than the value 0.94 shown in Figure 10(a).

In Figure 10(b) we compare the partition coefficients obtained from the simulations with the results predicted by Equation (25). The overestimation of size-exclusion effects found with the Carnahan-Starling equation for $g(\sigma)$ is again reflected in the lower K-values which this approximation provides. As expected, Equation (25) also fails to predict a percolation threshold which is a natural consequence of the allowed configurations in the random mixing statistics upon which this equation is based. A cavity connectedness function analogous to the particle pair connectedness function employed by Chiew *et al.* [8] and by other studies cited therein would need to be analyzed in order to correct this deficiency in Equation (25).

3.2 Comparison of Results from Models (iii) and (iv)

The second set of runs conducted for the nonoverlapping spheres model were at a porosity $\psi = 0.644$. In this case a limited number of simulations for the random nonoverlapping system (model (iii)) were carried out primarily for qualitative comparison with the connected nonoverlapping structure (model (iv)) and the results obtained for both systems are presented in Tables 8 through 11 and in Figures 11 and 12.

The results given in Tables 8 and 9 for α and β in the long-time tails of the VACF demonstrate features similar to those observed in our earlier comparison of the random and connected overlapping systems at high porosities. For the random nonoverlapping structure the percolation threshold occurs at the lower value $\sigma_c \sim 0.625$ compared with the critical value $\sigma_c \sim 0.975$ for the connected system. The results obtained for α and β near the percolation threshold are also significantly smaller in the random system than in the connected system although these differences, particularly with regard to the values of β (1.51 (random) and 1.64 (connected)) are

Table 8 Parameters for the Long-Time Tails of the VACF. Random Nonoverlapping System ($\psi = 0.644$).

σ	Δt^{*a}	α^b	β^b
0.0	–	–	–
0.4	15–40	0.43(3)	1.66(2)
0.55	15–40	0.48(2)	1.51(1)
0.7	15–40	0.82(6)	1.68(2)
	100–3000	0.39(1)	1.55(1)

[a] As in Table 3. In this case the simulated mean free time and the Enskog mean free time calculated using the Carnahan-Starling equation were in good agreement (see Table 10).
[b] The second set of results for $\sigma = 0.7$ were obtained from a least-squares fit of $\ln D^*(t^*)$ to $\ln t^*$ (Figure 11).
[c] This run was of insufficient length to determine α and β.
The number of scatterers employed in each run was 256 and the number of configurations generated in each case was 1000. The total length of an individual trajectory was 16×10^3 Enskog mean free times.

not nearly as large as in the overlapping systems. This suggests that solid phase connectivity has a weaker effect on the topology of the pore space in the nonoverlapping spheres model.

The last two sets of parameter values given in Tables 8 and 9 for $\sigma = 0.7$ and 1.05

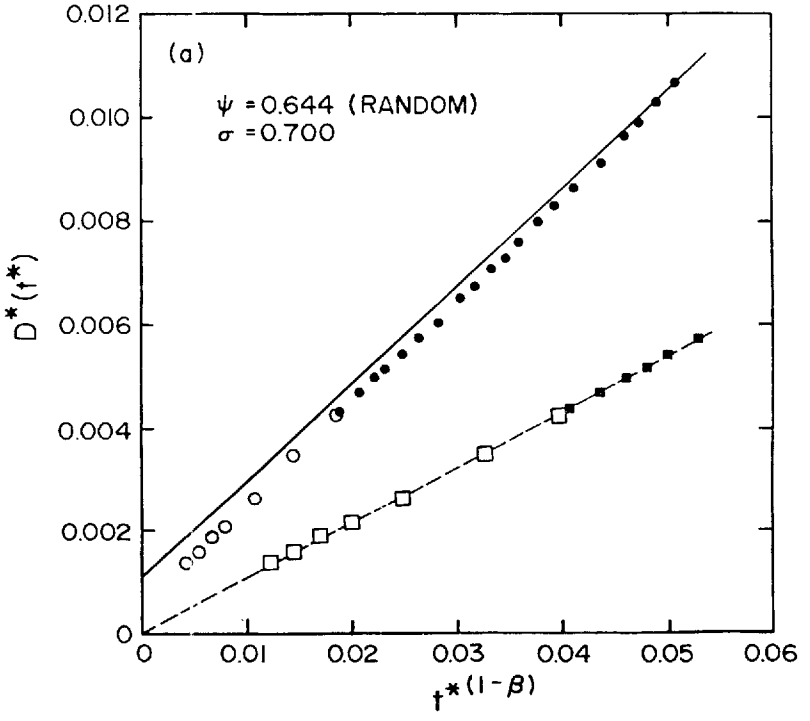

Figure 11 (a) $D^*(t^*)$ above the percolation threshold for the random nonoverlapping system ($\psi = 0.644$). The circles are the simulation results as a function of $t^{*1-\beta}$ with $\beta = 1.68$: ● VACF integration; ○ long-time slope of the mean square displacement; —— Equation (11) with $\beta = 1.68$, $\alpha = 0.82$. The squares are the same results plotted as a function of $t^{*(1-\beta)}$ with $\beta = 1.55$.

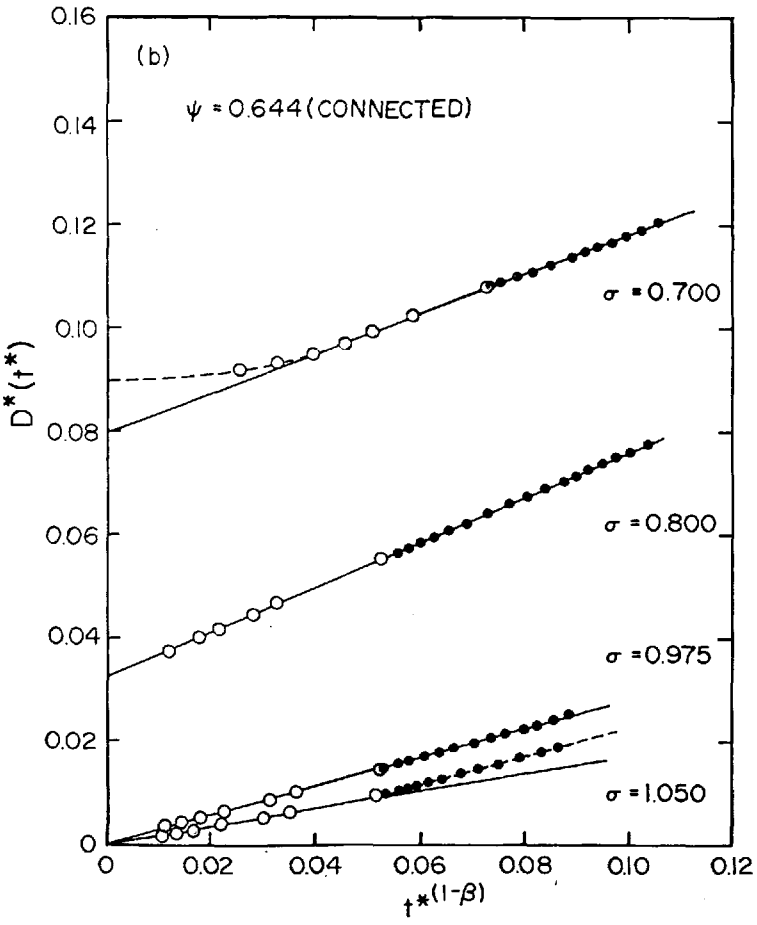

Figure 11 (b) $D^*(t^*)$ in the connected nonoverlapping system for several fluid particle sizes. The case $\sigma = 1.05$ is above the percolation threshold and the power law exponents are: $\beta = 1.64$ ($\sigma = 0.7$); 1.64 ($\sigma = 0.8$); 1.62 ($\sigma = 0.975$); $\beta = 1.65$ ($\sigma = 1.05$).

respectively also illustrate an effect briefly alluded to in the discussion of the connected overlapping system. Both of these particle sizes are above the respective percolation thresholds and in Figure 11 we can clearly see how the supercritical transition behaviour of the VACF can influence the correct extrapolation of $D(t^*)$ to find an infinite time diffusion coefficient equal to zero. The upper plot of full and open circles in Figure 11(a) is the time dependent diffusion coefficient expressed as a function of $t^{*(1-\beta)}$ with β given by the intermediate-time value 1.68. The accompanying solid line is Equation (11) with the same value of β and $\alpha = 0.82$ and we see that extrapolation of this line to infinite time gives an incorrect (positive) value for D^*. A transition from the power law exponent of 1.68 to a lower value at long times is however indicated at $t^* \sim 90$ and the squares shown in Figure 11(a) are the long-time results for $D^*(t^*)$ in the time range $200 < t^* < 3000$ replotted as a function of $t^{*(1-\beta)}$ with $\beta = 1.55$. The results given in Table 9 and plotted in Figure 11(b) for $\sigma = 1.05$ in the connected

Table 9 Parameters for the Long-Time Tails of the VACF. Connected Nonoverlapping System ($\psi = 0.644$)

σ	Δt^{*a}	α^b	β^b
0.0	-	-	-
0.3	11–28	0.55(4)	1.97(3)
0.45	11–28	0.62(5)	1.87(3)
0.7	15–50	0.68(6)	1.64(2)
0.8	15–50	0.87(7)	1.64(2)
0.9	15–50	0.9(1)	1.65(4)
0.975	15–50	0.7(1)	1.62(4)
1.05	15–50	1.2(3)	1.82(7)
	100–1150	0.44(5)	1.65(2)

[a] As in Table 3. The results for t^* relative to the Enskog mean free time estimated using the Carnahan-Sterling equation are given in Table 11.

[b] The second set of results for $\sigma = 1.05$ were obtained from a least-squares fit of $\ln D^*(t^*)$ to $\ln t^*$.

The number of scatterers employed in each run was 450 ± 5 (see the Appendix for details) and the number of configurations in each case was 1000. The total length of the individual trajectories was $16 \times 10^3 \tau_E^*(\text{C-S})$ where $\tau_E^*(\text{C-S})$ is given by Equations (22) and (23).

system further emphasize this behaviour. In this case the power law changes from $\beta = 1.82$ to 1.65 at $t^* \sim 100$ and the straight line represents a fit of $D^*(t^*)$ to $t^{*(1-\beta)}$ with $\beta = 1.65$ in the range $100 < t^* < 1150$. In both the random and connected systems we also observe that the transition of the tail of the VACF to a power law characteristic of the percolation threshold is accompanied by a significant lowering in the magnitude of α. The manner in which α varies through the transition region is most clearly seen from the results for the connected system in Table 9. In the subcritical anomalous diffusion regime α increases from a value of 0.68 to a maximum of 0.9 and then drops to 0.7 at the percolation threshold. Above the percolation threshold the long-time value for α continues its downward trend and we can surmise that it eventually goes to zero for large enough σ.

Although the only theoretical results currently available for the supercritical region pertain to the random overlapping system [31, 32], we may assume that these results should at least qualitatively apply to other structures. In the supercritical region Gotze *et al.* [31, 32] predict that both α and β will increase from their values at the percolation threshold as the scatterer density (or conversely the diffusing particle size σ) is increased. This is indeed what we observe for the intermediate-time tail parameters given in Tables 8 and 9. However, the inference from theory is that this trend in α and β refers to the tail of the VACF at very long times and this is contrary to the results obtained from the simulations. Our only conclusion at the present time is that while the theory of Gotze *et al.* is qualitatively correct in its prediction of the properties of the Lorentz gas below the percolation threshold, serious inconsistencies arise in the supercritical region.

The long-time properties determined for the random and connected nonoverlapping systems are given in Tables 10 and 11 respectively. For the random system at $\psi = 0.644$ the Enskog mean free times calculated using the Carnahan-Starling equation for $g(\sigma)$ are seen to be in excellent agreement with the simulation values. This is not true for the connected system except for $\sigma = 0$ where $g(\sigma = 0) = 1/\psi$ is exact regardless of the topology of the nonoverlapping structure. For $\sigma > 0$ the mean free times and free trajectory lengths are significantly larger in the connected spheres model for reasons similar to those given earlier for the connected overlapping system. The increase in size of the percolating cavities in going from the random to the

Table 10 Simulation Results for the Random Nonoverlapping System ($\psi = 0.644$).

σ	D^{*a}	P^b	K_T^b	R_P^{*b}	$\tau_c^*/\tau_E^*(C\text{-}S)^b$
0.0	0.761(1)	1.0	1.0	1.266	1.000(2)
0.4	0.1214(6)	1.0	0.283(5)	0.427	1.01(1)
0.55	‡0.0260(4)	0.993(3)	0.121(3)	0.316	1.00(1)
0.7	0	(0.048)	0.038(2)	0.244	0.99(5)

[a] As in Table 2.
[b] As in Tables 4 and 7.
‡ The time dependence of D^* for $\sigma = 0.55$ was found to by hydrodynamic for times greater than $t^* = 300$. The run for $\sigma = 0.7$ is above the percolation threshold.

Table 11 Simulation Results for the Connected Nonoverlapping System ($\psi = 0.644$)

α	D^{*a}	P^b	K_T^b	R_P^{*b}	$\tau_c^*/\tau_E^*(C\text{-}S)^b$
0.0	0.774(2)	1.0	1.0	1.264	1.007(4)
0.3	0.322(2)	1.0	0.554(8)	0.921	1.84(3)
0.45	0.231(1)	1.0	0.390(7)	0.781	2.22(2)
0.7	0.090(1)	1.0	0.184(6)	0.512	2.36(6)
0.8	‡0.033(1)	1.000(4)	0.124(4)	0.430	2.36(9)
0.9	‡0.0068(4)	0.84(12)	0.079(5)	0.383	2.5(1)
0.975	‡ −0.0006(8)	(0.17)	0.057(4)	0.376	2.8(1)
1.05	‡0	(0.049)	0.040(3)	0.368	3.0(2)

[a] As in Table 2.
[b] As in Tables 4 and 7. All time scales in Table 9 and Figure 11(b) are in units of τ_c^*.
‡ These diffusion coefficients were obtained by extrapolating the long-time tails given in Table 9. The run for $\sigma = 1.05$ is above the percolation threshold.

connected structure is also somewhat similar to the result observed in the overlapping models although the change is not as large in the present case.

In Figure 12(a) the diffusion coefficients relative to the point particle Enskog value are plotted as a function of diffusing particle size. The dashed line in this figure represents the results predicted by Enskog's theory for $\sigma > 0$ and should be compared with the simulation data for the random system (open circles). The apparent compatability of this theory with the results obtained for the connected system in the range $0 < \sigma < 0.5$ is fortuitous although we do note the very good agreement between the random system and connected system diffusion coefficients and D_E at $\sigma = 0$. As σ is increased we observe the expected increase in the relative magnitude of D in the connected structure with a significant shift in the position of the percolation threshold as indicated by the arrows.

In comparing the results shown in Figure 12(a) with the corresponding values in Figure 7(a) for the overlapping systems, we see that the most important differences occur at or near the percolation threshold. Since the magnitude of $D_E^{(0)}$ in Figure 12(a) is $\sim D^{(0)}$ we find that the diffusion coefficients within nonoverlapping structures are typically lower than those in overlapping systems at the same value of λ in the transition region. This observation and the lower percolation thresholds obtained in the nonoverlapping models reflect the influence of density fluctuations which are broader in overlapping sphere assemblies and hence allow for a wider range in pore sizes. For smaller particle sizes however the distinction between both types of models is minor. To illustrate this we can reconsider the experimental data obtained by Schneider and Smith [50] and Gangwal *et al.* [51] for diffusion of ethane and methane in microporous silica gel. Here we only estimate the "tortuosity" factors for the

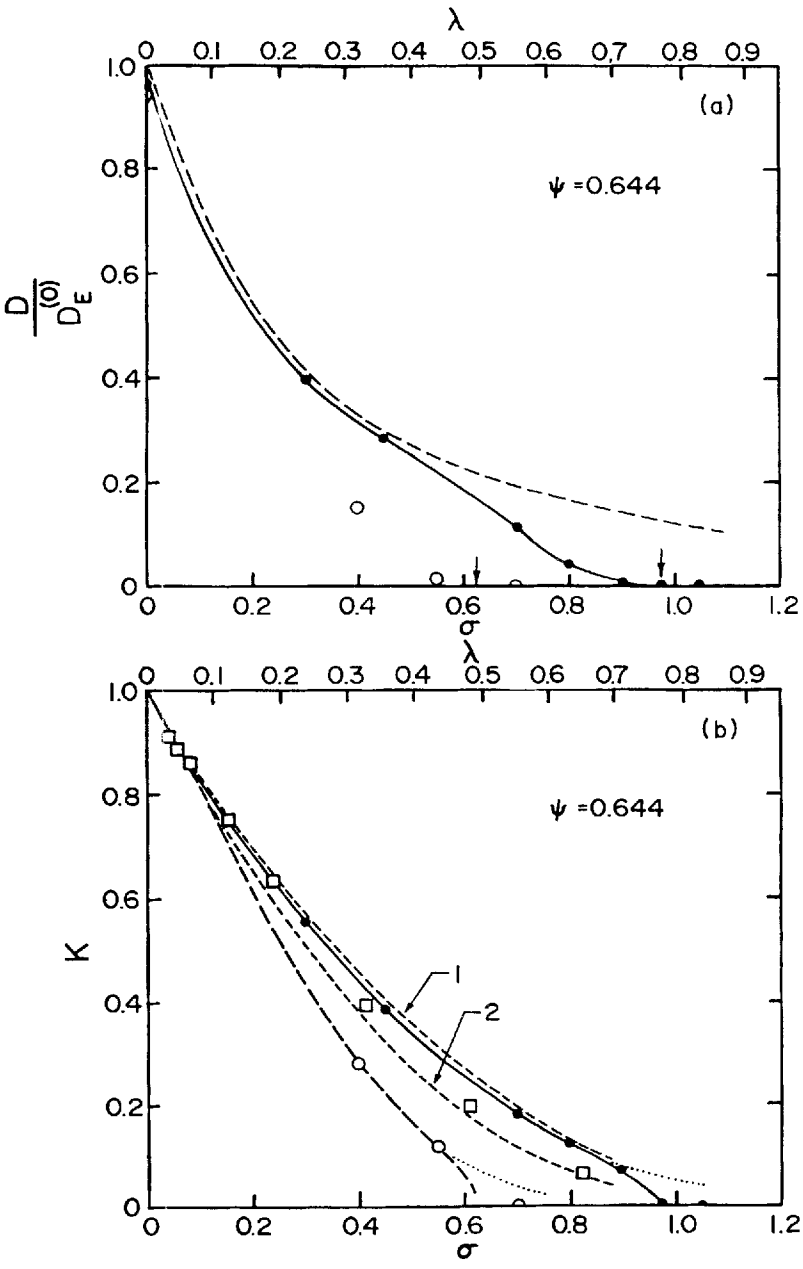

Figure 12 Diffusion and partitioning in nonoverlapping spheres models ($\psi = 0.644$).
(a) As in Figure 10. —— ● ——, ○ MD simulation for the connected and random structures respectively; – – – – Enskog equation. The arrows indicate the approximate position of the percolation thresholds in both cases.
(b)All symbols are as in figure 7(b). The Carnahan-Starling equation (equation (25)) coincides with the results for the random system, trapping regions included.

connected nonoverlapping system since the simulation results in this case are more complete.

To determine the total porosity of the silica gel and the partition coefficient of helium in the connected nonoverlapping spheres model, we observe from the results given in Tables 7 and 11 that the partition coefficient K_T at any given value of λ in the range $\lambda < 0.5$ is essentially independent of porosity. Therefore, using Figure 12(b) and the initial values $\psi = 0.49$ and $R_p = 11$ Å with $\sigma_{He} = 1.09$ Å [52], we find that the partition coefficient of helium is $K_{He} = 0.83$ and the true porosity is $\psi = 0.49/K_{He} = 0.59$ (note the agreement with the connected overlapping spheres model). From Figure 12(b) we also find that the partition coefficient for methane is $0.71(\lambda = 0.144)$ and for ethane is $0.64(\lambda = 0.181)$. Furthermore, when the ratio $D/D^{(0)}$ obtained from Tables 7 and 11 is reconsidered as a function of λ, it is found that the results for this ratio at any given value of λ do not deviate by more than 10% in the range $0 < \lambda < 0.3$. Since the porosity $\psi = 0.59$ is quite close to the value upon which Figure 12(a) is based, we may therefore use this figure to estimate $D/D^{(0)}$ with reasonable accuracy ($\lesssim 2\%$ error). The values of $D/D^{(0)}$ so determined are 0.57 (methane) and 0.50 (ethane), which are approximately 6% lower than the corresponding results for the connected overlapping system. Finally we note from the results given in Tables 7, 10 and 11 that for point particles the ratio D^*/R_p^* is, with little error, independent of both the topology and the porosity of the medium. Using the value $D^*/R_p^*(\sigma = 0) = 0.61$ at $\psi = 0.644$ and the preceding estimates for K and $D/D^{(0)}$ then the "tortuosities" predicted by Equation (21) for the connected nonoverlapping spheres model are 2.68 (methane) and 3.39 (ethane), both of which are in good agreement with the experimental values 2.4 and 3.35 respectively. These results in fact suggest that the connected nonoverlapping spheres model better represents the structure of silica gel than the overlapping model and indicate that the colloidal silica particles formed during the manufacture of the gel do not interpenetrate one another.

In Figure 12(b) we plot the partition coefficients obtained for both the random and connected nonoverlapping systems. In this case, as with $g(\sigma)$, the partition coefficients predicted by the Carnahan-Starling equation (Equation (25)) for the random model are in very good agreement with the simulation results for K_T. Also shown in this figure are the experimental data obtained by van Kreveld and van den Hoed [44] plotted as a function of $\lambda = R_g/R_p(\sigma = 0)$. These data are again seen to scatter around the simulation results for the connected system although we observe much better agreement with the simulations at low values of λ. For $\lambda \geqslant 0.3$ the data tend to deviate towards the theoretical results predicted by Equation (17) and we believe this provides strong support for the contention that coil configurations in the polystyrene macromolecules are a dominant factor in very small pores. We also note the suprisingly good agreement between the simple expression given in Equation (18) and the K-values obtained for the connected model. This observation and the trends in the data of van Kreveld and van den Hoed suggest that the connected nonoverlapping structure may also be an improvement over the overlapping model as a description for the solid phase of Porasil C.

Before concluding, it is worthwhile to briefly consider one further aspect inferred by the results for β given in Tables 6, 8 and 9. For percolation on a lattice we have already noted in Section 2 that the value of β is 1.59 in agreement with the result obtained for the random overlapping system. For the connected overlapping system at high porosity the power law exponent was found to be more appropriate to a randomly branched pore structure. In the case of the nonoverlapping systems how-

ever none of the values obtained for β conform with lattice percolation theory. Unfortunately, the limited amount of data obtained here for the percolation probabilities and the diffusion coefficients in the subcritical anomalous diffusion regime do not permit estimation of the parameters μ and γ in Equation (12) and (16) and for this reason we can provide no explanation for the low values of β observed in the RCP and random nonoverlapping structures (except possibly with regard to the importance of ring collisional events mentioned earlier). However, the larger value of $\beta = 1.64$ in the high porosity connected system may be indicative of a tree-like pore structure which is qualitatively similar to that of the connected overlapping model at the same porosity. In view of our definition of connectivity in the nonoverlapping system (i.e. the RCP structure is considered to be naturally connected), the large increase in β in going from $\psi = 0.367$ to $\psi = 0.644$ also suggests that β will continue to increase for porosities greater than 0.644 thus emphasizing the possible role of pore branching.

4 SUMMARY AND CONCLUSION

The appeal of random sphere models of porous media lies in their simplicity and in their ability to provide a framework within which one may investigate the properties of fluids in amorphous materials while at the same time incorporating a rational approach to the structure of the solid phase. Current models in this area are however limited with regard to their treatment of the topology of the solid. It has been one of the objectives of this paper to demonstrate the importance of bicontinuity of the solid and pore phases in random assemblies of solid spheres particularly when the pores and fluid particles have dimensions of commensurate size.

A comparison of the simulation results obtained for the connected overlapping and nonoverlapping models with available experimental data on partitioning and diffusion in porous materials has shown that these structures are better representations of the solid (inclusion) phase than completely random models. In the two cases considered (Porasil C [44] and silica gel [50, 51]) it was found that the connected nonoverlapping spheres structure provided better agreement with the data than the connected overlapping system, in support of its applicability as a model for porous solids formed from colloidal suspensions as well as pelletized or mildly sintered particle packings. This does not however preclude the possibility that the overlapping system may provide a better description of other media particularly at low porosities or for systems that exhibit a strong ψ-dependence of the free molecule diffusion coefficient $D^*(\sigma = 0)$. From an analysis of the long-time tails of the VACF we also found that constrained connectivity in random sphere assemblies radically influences the pore space percolation properties as the porosity is increased above $\psi = 0.5$. Under these conditions the power law exponent on the VACF tail increases significantly and the geometric properties of the pores display characteristics akin to a randomly branched structure, particularly in the case of the connected overlapping spheres model, with large cavities similar to those inferred from the hysteresis loops of adsorption/desorption isotherms.

The simulation results obtained for the time-dependent properties of the pore fluid also enabled a detailed comparison with current theories of diffusion in Lorentz gases. In particular we have shown that the mode-coupling method of Ernst *et al.* [34, 35] is qualitatively correct in its assessment of the magnitude of the hydrodynamic tail of

the VACF although much work still needs to be done. In the vicinity of the percolation transition the theory of Gotze *et al.* [31, 32] under subcritical conditions is also qualitatively supported by our results. This theory and the kinetic studies of Masters and Keyes [33] emphasize the existence of hydrodynamic effects at very long times and these were indeed found to have an important bearing on the evaluation of the infinite-time diffusion coefficients near the percolation threshold. In the supercritical regime however, inconsistencies appear to arise in the theoretical results predicted by Gotze *et al.* and futher studies in this area are clearly needed.

Acknowledgments

The authors gratefully acknowledge the financial support of the National Science Foundation (Grant CBT-8505246) and the technical assistance of the University of Missouri-Rolla Computer Center and the National Center for Supercomputing Applications, Urbana-Champaign, Illinois. We also wish to acknowledge Dr. S.-H. Suh for preliminary work on the coding of the molecular dynamics algorithm.

APPENDIX

In most of the computations we have employed standard simulation techniques with minor modifications which we briefly outline here. The random overlapping spheres structures were generated by random placement of spheres in fundamental cells of side-length L^*, the latter being determined both by the desired porosity and number of scatterers (Table 1) using Equation (7). In generating the connected overlapping structures we used the cluster labeling algorithm described by Hoshen and Kopelman [65] and Gawlinski and Stanley [66]. These computations involved random placement of the spheres with sequential labeling and scanning for overlapping neighborhood particles as each new sphere was added. After addition of a preset number of scatterers, corresponding to a porosity slightly lower than the final desired porosity of the connected structure, the cluster labels assigned to each particle and the number of particles belonging to each cluster are stored in two vector arrays. A straightforward search provides the largest cluster and a sorting routine reassigns the particle coordinates in this cluster in a sequential manner. The particles in the smaller clusters are then discarded. The large cluster is checked for sample spanning between the faces of the fundamental cell in one or more of the x, y and z directions (connectivity with at least one image particle in opposite faces of the cell was used as a criterion for sample spanning). Once sample spanning has been verified new particles are randomly added to the cluster to bring the porosity of the cell to its desired value. In operation it took approximately 0.2 sec or less to generate a single configuration for the connected overlapping system at $\psi = 0.644$ on a Cray-XMP computer. To obtain this porosity and a final particle number $N_s = 400$, the initial porosity of the labelled random systems was chosen to be 0.61 and a few trial configurations indicated that a side-length for the cell $L^* = 15.316$ would give a connected system with $\psi = 0.644$. During the cluster search only those large clusters containing between 350 to 400 particles were chosen as the backbone for the connected system. Subsequent filling of the cell to give $N_s = 400$ in 1500 configurations gave an ensemble average porosity of $\psi = 0.644 \pm 1\%$. Similarly, for the connected overlapping system at $\psi = 0.59 \pm 1\%$ it was found that a fundamental cell of side-length $L^* = 14.467$

would accommodate 400 connected spheres with the initial porosity of the labelled random systems taken as 0.56.

The random close-packed nonoverlapping system was generated using the procedure described by Mason [18]. Two prototype systems were constructed, one containing 200 scatterers and the second containing 800 scatterers. The first system was employed as the "seed" configuration in the simulations on the RCP structure reported in the paper. Each new configuration of the 1500 generated was obtained after 2×10^5 trial moves in the Monte Carlo procedure of Metropolis *et al.* [67]. A significant savings in CPU time was achieved by using a neighborhood list of the shell particles surrounding any given particle since the same nearest neighbors were always involved at the high density corresponding to $\psi = 0.367$ [68]. The configurations for the nonoverlapping connected system at the porosity $\psi = 0.644$ were generated using the 800 particle RCP "seed" configuration. In this case 200 new RCP configurations were obtained during the course of 3.2×10^7 Monte Carlo trial moves on the original structure. From each of these configurations five connected systems were generated giving a total of 1000 connected configurations. The manner in which the individual connected sphere assemblies were obtained was similar to that described above for the overlapping system but with the following modifications. Contact connectivity of random nonoverlapping sphere assemblies is never assured in Monte Carlo simulations, and in order to define connectedness the solid phase percolation properties of the RCP configurations were examined by gradually increasing the size of the spheres. In all cases an increase of one percent or less in the diameter of the spheres resulted in complete connectivity. This expansion factor was used to define connected clusters at $\psi = 0.644$. An individual connected structure was generated by randomly removing 325 particles from one of the 200 RCP configurations containing 800 spheres. A cluster search using the expansion factor defined above and a labeling routine similar to that outlined earlier provided the largest connected cluster in the cell. Only those clusters containing between 445 and 455 particles were examined for sample spanning with the result that $\psi = 0.644 \pm 1\%$ for the ensemble of configurations.

Although the nonoverlapping systems described above are not truly connected we feel that for the purposes of demonstrating the influence of solid phase topology on partitioning and diffusion of fluid particles in the size range $0.3 \leqslant \sigma \leqslant 1.05$ (Tables 9 and 11) the effect of a separation distance $\leqslant 0.02$ between the surfaces of nearest neighbour solid spheres is negligible. The most time consuming part involved in the procedure was in generating the RCP configurations (~ 30 seconds per configuration on a Cray-XMP). The time required to obtain a connected nonoverlapping structure was comparable to that needed in the overlapping case.

The configurations for the random nonoverlapping system at $\psi = 0.644$ were generated from a face-centered cubic lattice using the standard Monte Carlo procedure of Metropolis *et al* [67]. The initial FCC structure was chosen for its "looseness" and to provide an unbiased comparison with the connected system at the same porosity.

The molecular dynamics procedure employed to determine the time dependent properties and the diffusion coefficients reported in this paper was the same as that described by Bruin [22] and the reader is referred to that source for details. Apart from differences in the underlying structure of the scattering medium the only major difference in our work is the length of the individual trajectories which were between 2×10^3 and 16×10^3 mean-free times long. Our reasons for computing trajectories of this length were twofold: (i) to obtain improved statistics and (ii) to determine

percolation probabilities in a manner similar to that outlined by Nakano and Evans [6]. This procedure entails tracking the distance travelled by a given particle from its origin. If this distance should equal the side-length of the fundamental cell in either the x, y, or z directions at any time during the trajectory than the original starting point of the particle is considered to be in the open pore space of the medium. The number of percolating trajectories were counted during the course of a given run and the times taken for the particles to diffuse across the fundamental cell were recorded. A typical plot of the distribution of trajectory times displayed a peak at intermediate times followed by an exponential decay at very long times. To estimate the number of trajectories which would have eventually proven to be percolating the tail of this distribution was fitted to an exponential. The number of these trajectories was usually a small percentage of the total number actually recorded during the simulation except at the percolation threshold where, as we have noted in the paper, the influence of system size severely limits the reliability of this method.

The two remaining quantities calculated were the average pore radii and the partition coefficients. The average pore radii were determined during the MD simulations and simply correspond to one half the average length of the free particle trajectories between successive collisions with the scattering centers. The partition coefficients were determined using a standard Monte Carlo insertion technique. 10^3 trial insertions were carried out on each configuration and for each particle size recorded in the main text as well as for other particle sizes in order to obtain K as a function of σ. This method provides the total partition coefficient and does not differentiate between closed and open pore regions. In the vicinity of the percolation threshold the results shown in Figures 7(b), 10(b), and 12(b) were obtained by multiplying the total partition coefficients by the percolation probabilities.

With the exception of a few runs for the random overlapping system and the connected overlapping system ($\psi = 0.59$) which were carried out on an FPS-164 computer, all of the results presented here were obtained using the Cray-XMP supercomputer at the National Center for Supercomputing Applications, Urbana-Champaign, Illinois.

References

[1] S. Reyes and K.F. Jensen, "Estimation of Effective Transport Coefficients in Porous Solids Based on Percolation Concepts", *Chem. Eng. Sci.*, **40,** 1723 (1985).
[2] S. Prager, "Diffusion and Viscous Flow in Concentrated Suspensions", *Physica*, **29,** 129 (1963).
[3] H.L. Weissberg, "Effective Diffusion Coefficient in Porous Media", *J. Appl. Phys.*, **34,** 2636 (1963).
[4] H.A.M. van Eekelen, "The Random-Spheres Model for Porous Materials", *J. Catal.*, **29,** 75 (1973).
[5] F.G. Ho and W. Strieder, "Numerical Evaluation of the Porous Medium Effective Diffusivity Between the Knudsen and Continuum Limits", *J. Chem. Phys.*, **73,** 6296 (1980).
[6] Y. Nakano and J.W. Evans, "Monte Carlo Simulation of Diffusion of Gases in a Porous Solid: Calculations for a New Class of Solids", *J. Chem. Phys.*, **78,** 2568 (1983).
[7] M.H. Abbasi, J.W. Evans, and I.S. Abramson, "Diffusion of Gases in Porous Solids: Monte Carlo Simulations in the Knudsen and Ordinary Diffusion Regimes", *AIChE J.*, **29,** 617 (1983).
[8] Y.C. Chiew, G. Stell, and E.D. Glandt, "Clustering and Percolation in Multicomponent Systems of Randomly Centered and Permeable Spheres", *J. Chem. Phys.*, **83,** 761 (1985).
[9] J.M. Haile, C. Massobrio and S. Torquato, "Two-Point Matrix Probability Function for Two-Phase Random Media: Computer Simulation Results for Inpenetrable Spheres", *J. Chem. Phys.*, **83,** 4075 (1985).
[10] J.M.D. MacElroy and J.J. Kelly, "Hindered Diffusion of Gases in "Leaky" Membranes Using the Dusty Gas Model", *AIChE J.*, **31,** 34 (1985).
[11] P.A. Rikvold and G. Stell, "D-Dimensional Interpenetrable-Spheres Models of Random Two-Phase Media: Microstructure and an Application to Chromatography", *J. Colloid Interface Sci.*, **108,** 158 (1985).

[12] N.A. Seaton and E.D. Glandt, "Spatial Correlation Functions from Computer Simulations", *J. Chem. Phys.*, **85,** 5262 (1986).
[13] S. Torquato, "Microstructure Characterization and Bulk Properties of Disordered Two-Phase Media", *J. Stat. Phys.*, **45,** 843 (1986).
[14] V.K.S. Shante and S. Kirkpatrick, "An Introduction to Percolation Theory", *Adv. Phys.*, **20,** 325 (1971).
[15] S. Kirkpatrick, "Percolation and Conduction", *Rev. Mod. Phys.*, **45,** 574 (1973).
[16] S.W. Haan and R. Zwanzig, "Series Expansions in a Continuum Percolation Problem", *J. Phys. A: Math. Gen.*, **10,** 1547 (1977).
[17] J.D. Bernal, "The Structure of Liquids", *Proc. Roy. Soc. (Lond.)*, **A280,** 299 (1964).
[18] G. Mason, *Disc. Faraday Soc.*, **43,** 75 (1967).
[19] J.L. Finney, "Random Packings and the Structure of Simple Liquids. I. The Geometry of Random Close Packing", *Proc. Roy. Soc. (Lond.)*, **A319,** 479 (1970).
[20] D.P. Haughey and G.S.G. Beveridge, "Structural Properties of Packed Beds – A Review", *Can. J. Chem. Eng.*, **47,** 130 (1969).
[21] For reviews of work in this area see E.H. Hauge, "What Can One Learn from Lorentz Models?" in *Transport Phenomena*, G. Kirczenow and J. Marro (Eds.) Lecture Notes in Physics, Springer, Berlin, **31**, 337 (1974); H. van Beijeren, "Transport Properties of Stochastic Lorentz Models", *Rev. Mod. Phys.*, **54**, 195 (1982).
[22] C. Bruin, "A Computer Experiment on Diffusion in the Lorentz Gas", Delft University Press (1978).
[23] J. Courtenay Lewis and J.A. Tjon, "Evidence for Slowly-Decaying Tails in the Velocity Autocorrelation Function of a Two-Dimensional Lorentz Gas", *Phys. Lett.*, **66A,** 349 (1978).
[24] W.E. Alley, "Studies in Molecular Dynamics of the Friction Coefficient and the Lorentz Gas", Ph.D. Thesis, University of California, Davis (1979).
[25] B.J. Alder and W.E Alley, "The Lorentz Gas", in *Studies in Statistical Mechanics, IX, Perspectives in Statistical Physics*, H.J. Raveche, E.W. Montroll and J.L. Lebowitz (Eds.), North-Holland Publ. Co., Amsterdam (1981).
[26] B.J. Alder and W.E. Alley, "Decay of Correlations in the Lorentz Gas", *Physica*, **121A,** 523 (1983).
[27] C.P. James and G.T. Evans, "Diffusion in the Two-Dimensional Nonoverlapping Lorentz Gas", *J. Chem. Phys.*, **87,** 4056 (1987).
[28] J.M.J. van Leeuwen and A. Weijland, "Non-Analytic Density Behaviour of the Diffusion Coefficient of a Lorentz Gas. I. Divergencies in the Expansion in Powers in the Density", *Physica*, **36,** 457 (1967).
[29] A. Weijland and J.M.J. van Leeuwen, "Non-Analytic Density Behaviour of the Diffusion Coefficient of a Lorentz Gas. II. Renormalization of the Divergencies", *Physica*, **38,** 35 (1968).
[30] T. Keyes and J. Mercer, "Some Considerations on the Calculation of the Velocity Correlation Function in the Ring Approximation, with Application to the Lorentz Gas", *Physica*, **95A,** 473 (1979).
[31] W. Gotze, E. Leutheusser, and S. Yip, "Dynamical Theory of Diffusion and Localization in a Random, Static Field", *Phys. Rev. A*, **23,** 2634 (1981).
[32] W. Gotze, E. Leutheusser, and S. Yip, "Correlation Functions of the Hard-Sphere Lorentz Model", *Phys. Rev. A*, **24,** 1008 (1981).
[33] A. Masters and T. Keyes, "Diffusion, Percolation, and Trapping in the Lorentz Gas via Variational Kinetic Theory", *Phys. Rev. A*, **26,** 2129 (1982).
[34] M.H. Ernst, J. Machta, J.R. Dorfman, and H. van Beijeren, "Long Time Tails in Stationary Random Media. I. Theory", *J. Stat. Phys.*, **34,** 477 (1984).
[35] J. Machta, M.H. Ernst, H. van Beijeren, and J.R. Dorfman, "Long-Time Tails in Stationary Random Media. II. Applications." *J. Stat. Phys.*, **35,** 413 (1984).
[36] B.J. Berne, "Time-Dependent Properties of Condensed Media", Ch. 9 in *Physical Chemistry – An Advanced Treatise*, Vol. 8B, D. Henderson (Ed.), Academic Press, N.Y. (1971).
[37] B.D. Hughes and B.W. Ninham (Eds.), *The Mathematics and Physics of Disordered Media*, Lecture Notes in Mathematics, 1035, Spinger, Berlin (1983).
[38] J. Kertesz, "Percolation of Holes Between Overlapping Spheres: Monte Carlo Calculation of the Critical Volume Fraction", *J. Phys. Lett.*, **42,** L393 (1981).
[39] J. Machta and S.M. Moore, "Diffusion and Long-Time Tails in the Overlapping Lorentz Gas", *Phys. Rev. A*, **32,** 3164 (1985).
[40] Y. Gefen, A. Aharony, and S. Alexander, "Anomalous Diffusion on Percolating Clusters", *Phys. Rev. Lett.*, **50,** 77 (1983).
[41] T. Keyes, "Divergences in the Amplitudes of the "Long-Time Tails", *Phys. Rev. A*, **29,** 415 (1984).
[42] W.T. Elam, A.R. Kerstein and J.J. Rehr, "Critical Properties of the Void Percolation Problem for Spheres", *Phys. Rev. Lett.*, **52,** 1516 (1984).

[43] M. Sahimi, "Critical Exponents and Thresholds for Percolation and Conduction", in *The Mathematics and Physics of Disordered Media*, B.D. Hughes and B.W. Ninham (Eds.), Lecture Notes in Mathematics, 1035 Springer, Berlin (1983).
[44] M.E. van Kreveld and N. van den Hoed, "Mechanism of Gel Permeation Chromatography: Distribution Coefficient", *J. Chromatography*, **83,** 111 (1973).
[45] C.K. Colton, C.N. Satterfield, and C.-J. Lai, "Diffusion and Partitioning of Macromolecules within Finely Porous Glass", *AIChE J.*, **21**, 289 (1975).
[46] C.N. Satterfield, C.K. Colton, B. de Turckheim, and T.M. Copeland, "Effect of Concentration on Partitioning of Polystyrene within Finely Porous Glass", *AIChE J.*, **24,** 937 (1978).
[47] R.E. Baltus and J.L. Anderson, "Hindered Diffusion of Asphaltenes through Microporous Membranes", *Chem. Eng. Sci.*, **38,** 1959 (1983).
[48] E.F. Casassa, "Equilibrium Distribution of Flexible Polymer Chains Between a Macroscopic Solution Phase and Small Voids", *J. Polym. Sci.*, Part B, **5** 773 (1967).
[49] E.F. Casassa and Y. Tagami, "An Equlibrium Theory for Exclusion Chromatography of Branched and Linear Chains", *Macromol.*, **2,** 14 (1969).
[50] P. Schneider and J.M. Smith, "Chromatographic Study of Surface Diffusion", *AIChE J.* **14,** 886 (1968).
[51] S.K. Gangwal, R.R. Hudgins, and P.L. Silveston, "Reliability and Limitations of Pulse Chromatography in Evaluating Properties of Flow Systems. I. Modelling and Experimental Considerations", *Can. J. Chem. Eng.*, **57,** 609 (1979).
[52] S. Chapman and T.G. Cowling, *The Mathematical Theory of Non-Uniform Gases*, 3rd Ed., Cambridge Univ. Press (1970).
[53] B.V. Derjaguin, "Measurement of the Specific Surface Area of Porous and Disperse Bodies", *Dokl. An. S.S.S.R.*, **53,** 627 (1946).
[54] E.A. Mason and S. Chapman, "Motion of Small Suspended Particles in Nonuniform Gases", *J. Chem. Phys.*, **36,** 627 (1962).
[53] W.C. Strieder and S. Prager, "Knudsen Flow through a Porous Medium", *Phys. Fluids*, **11**, 2544 (1968).
[56] L. Monchick, K.S. Yun, and E.A. Mason, "Formal Kinetic Theory of Transport Phenomena in Polyatomic Gas Mixtures", *J. Chem. Phys.*, **39,** 654 (1963).
[57] N.G. Stanley-Wood and A. Chatterjee, "The Comparison of the Surface Area of Porous and Non-Porous Solids as Determined by Diffusional Flow and Nitrogen Adsorption", *Powder Technol.*, **9,** 7 (1974).
[58] B.V. Derjaguin, D.V. Fedoseev, and S.P. Vnukov, "Measurement of the Specific Surface of Powders by the Method of Filtering Rarified Gas", *Powder Technol.*, **14,** 169 (1976).
[59] S. Redner, "Directionality Effects in Percolation", in *the Mathematics and Physics of Disordered Media*, B.D. Hughes and B.W. Ninham (Eds.), Lecture Notes in Mathematics, 1035, Springer, Berlin (1983).
[60] B.G. Linsen and A. van den Heuvel, "Pore Structures", Ch. 35 in *The Solid-Gas Interface*, Vol. 2, E.A. Flood (Ed.), Marcel Dekker, Inc. N.Y. (1967).
[61] T.M. Reed and K.E. Gubbins, *Applied Statistical Mechanics*, McGraw-Hill Book Co., N.Y. (1973).
[62] R. Zallen, "Stochastic Geometry: Aspects of Amorphous Solids", in *Studies in Statistical Mechanics, Vol VII, Fluctuation Phenomena*, E.W. Montroll and J.L. Lebowitz (Eds.) North-Holland Publ. Co., Amsterdam (1979).
[63] B.J. Alder and T.E. Wainwright, "Studies in Molecular Dynamics. II. Behaviour of a Small Number of Elastic Spheres", *J. Chem. Phys.*, **33,** 1439 (1960).
[64] A.J. Masters and T. Keyes, "Variational Principle in Kinetic Theory: Repeated-ring Approximation for the Lorentz Gas", *Phys. Rev. A*, **25,** 1010 (1982).
[65] J. Hoshen and R. Kopelman, "Percolation and Cluster Distribution. I. Cluster Multiple Labeling Technique and Critical Concentration Algorithm", *Phys. Rev. B*, **14,** 3438 (1976).
[66] E.T. Gawlinski and H.E. Stanley, "Continuum Percolation in Two Dimensions: Monte Carlo Tests of Scaling and Universality for Non-Interacting Discs", *J. Phys. A*, **14,** ;L291 (1981).
[67] N. Metropolis, A.W. Rosenbluth, M.N. Rosenbluth, A.H. Teller, and E. Teller, "Equation of State Calculations by Fast Computing Machines", *J. Chem. Phys.*, **21,** 1087 (1953).
[68] M.N. Rosenbluth and A.W. Rosenbluth, "Further Results on Monte Carlo Equations of State", *J. Chem. Phys.*, **22**, 881 (1954).